Title

Acute post-injury blockade of α2δ-1 calcium channel subunits prevents pathological autonomic plasticity after spinal cord injury

Journal

Cell Reports, 34(4)

ISSN

2639-1856

Authors

Brennan, Faith H
Noble, Benjamin T
Wang, Yan
et al.

Publication Date

2021

DOI

10.1016/j.celrep.2020.108667

Peer reviewed

HHS Public Access

Author manuscript

Cell Rep. Author manuscript; available in PMC 2022 February 05.

Published in final edited form as:

Cell Rep. 2021 January 26; 34(4): 108667. doi:10.1016/j.celrep.2020.108667.

Acute post-injury blockade of α2δ−1 calcium channel subunits prevents pathological autonomic plasticity after spinal cord injury

Faith H. Brennan[1,7], **Benjamin T. Noble**[1,7], **Yan Wang**[1,7], **Zhen Guan**[1], **Hayes Davis**[1], **Xiaokui Mo**[2], **Clay Harris**[3], **Cagla Eroglu**[4], **Adam R. Ferguson**[5,6], **Phillip G. Popovich**[1,8,*]

[1]Department of Neuroscience, Belford Center for Spinal Cord Injury, The Ohio State University, Columbus, OH 43210, USA

[2]Center for Biomedical Informatics, The Ohio State University, Columbus, OH 43210, USA

[3]Department of Chemistry and Biochemistry, The Ohio State University, Columbus, OH 43210, USA

[4]Department of Cell Biology, Duke University Medical Center, and Duke Institute for Brain Sciences, Durham, NC 27710, USA

[5]Brain and Spinal Injury Center (BASIC), Department of Neurological Surgery, Weill Institute for Neurosciences, University of California, San Francisco (UCSF), San Francisco, CA 94142, USA

[6]San Francisco Veterans Affairs Healthcare System (SFVAHCS), San Francisco, CA, USA

[7]These authors contributed equally

[8]Lead contact

SUMMARY

After spinal cord injury (SCI), normally innocuous visceral or somatic stimuli can trigger uncontrolled reflex activation of sympathetic circuitry, causing pathological dysautonomia. We show that remarkable structural remodeling and plasticity occur within spinal autonomic circuitry, creating abnormal sympathetic reflexes that promote dysautonomia. However, when mice are treated early after SCI with human-equivalent doses of the US Food and Drug Administration (FDA)-approved drug gabapentin (GBP), it is possible to block multi-segmental excitatory synaptogenesis and abolish sprouting of autonomic neurons that innervate immune organs and sensory afferents that trigger pain and autonomic dysreflexia (AD). This “prophylactic GBP” regimen decreases the frequency and severity of AD and protects against SCI-induced immune

*Correspondence: phillip.popovich@osumc.edu.

AUTHOR CONTRIBUTIONS

Conceptualization, P.G.P.; methodology, F.H.B., B.T.N., Y.W., A.R.F., and P.G.P.; investigation, F.H.B., B.T.N., Y.W., Z.G., H.D., A.R.F., X.M., and C.H.; writing – original draft, F.H.B., B.T.N., Y.W., C.E., and P.G.P.; writing – review & editing, F.H.B., B.T.N., A.R.F., and P.G.P; C.E. provided α2δ−1 transgenic mice; visualization, F.H.B. and P.G.P.; funding, P.G.P.

DECLARATION OF INTERESTS

The authors declare no competing interests.

SUPPLEMENTAL INFORMATION

Supplemental Information can be found online at https://doi.org/10.1016/j.celrep.2020.108667.

suppression. These benefits persist even 1 month after stopping treatment. GBP could be repurposed to prevent dysautonomia in at-risk individuals with high-level SCI.

In Brief

Brennan et al. show that α2δ−1 calcium channel subunits drive remarkable structural reorganization of autonomic circuitry and autonomic dysfunction after spinal cord injury. Early (prophylactic) post-injury treatment with gabapentin, an FDA-approved drug, prevents α2δ−1-dependent structural changes and autonomic dysfunction. Prophylactic gabapentin could be repurposed clinically for at-risk individuals.

Graphical Abstract

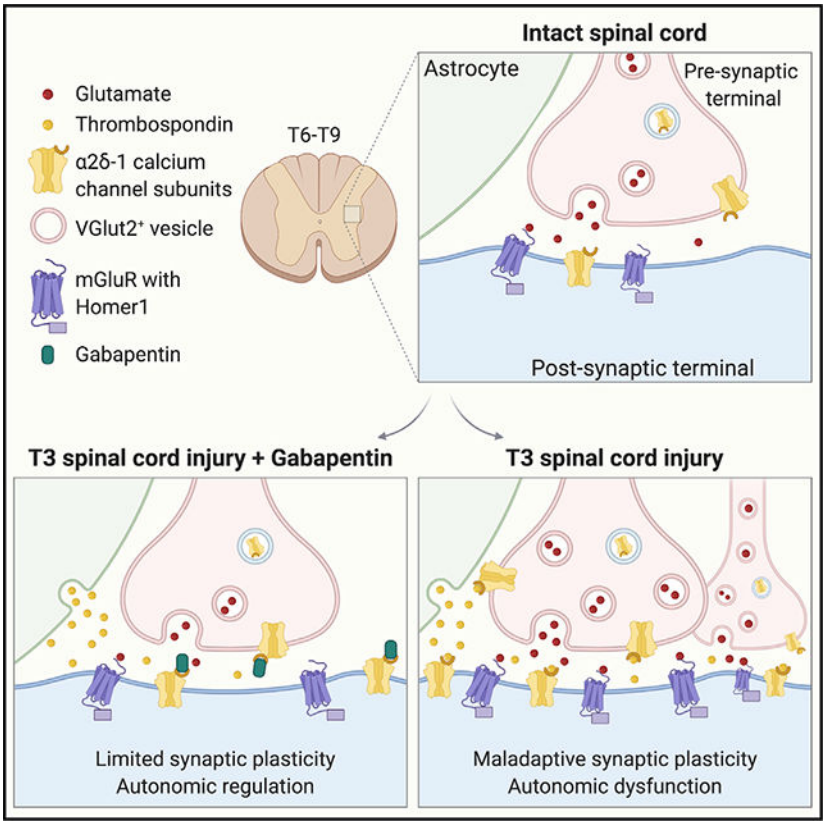

INTRODUCTION

Spinal cord injury (SCI) above spinal level T6 removes supraspinal control over sympathetic preganglionic neurons (SPNs) residing in the thoracic and upper lumbar spinal cord. As a result, normal visceral or somatic stimuli (e.g., distended bladder or bowel) below the lesion trigger uncontrolled reflex activation of sympathetic circuitry, leading to widespread dysautonomia that adversely affects multiple organs. The cardiovascular manifestation of dysautonomia is autonomic dysreflexia (AD), a hypertensive medical emergency that causes long-term health deficits (Guttmann and Whitteridge, 1947; Kursh et al., 1977). Sympathetic

hyperreflexia also causes immune suppression, which predisposes individuals to infection (Lucin et al., 2007, 2009; Prüss et al., 2017; Zhang et al., 2013).

Clinical and experimental data show that AD develops 1 week after high-level SCI and increases in frequency over time (Lindan et al., 1980; Mayorov et al., 2001; Zhang et al., 2013). This temporal escalation is presumably caused by remodeling of neuronal networks below the level of injury (Cameron et al., 2006; Llewellyn-Smith and Weaver, 2001; Llewellyn-Smith et al., 2006). Although independent studies have documented anatomical remodeling in sensory, motor, and autonomic circuits below the level of injury (Cameron et al., 2006; Krenz and Weaver, 1998; Sun et al., 2020; Ueno et al., 2016), the hypothesis that high-level SCI triggers progressive excitatory synaptogenesis caudal to the lesion, and a mechanistic explanation for this remodeling, remains untested.

After CNS injury, astrocytes and macrophages secrete thrombospondins (TSPs), a family of matricellular proteins that regulate the cell-cell and cell-matrix interactions required to stimulate synaptogenesis (Eroglu et al., 2009; Risher et al., 2018). Notably, TSPs bind neuronal α2δ−1 calcium channel subunits to promote excitatory synaptogenesis (Christopherson et al., 2005; Risher and Eroglu, 2012). If a similar mechanism is responsible for promoting new synapse formation in the distal spinal cord after injury, then drugs designed to block α2δ−1 calcium channel subunits should limit this structural plasticity.

Gabapentin (GBP), a US Food and Drug Administration (FDA)-approved drug used to treat neuropathic pain, binds α2δ calcium channel subunits (Field et al., 2006; Gee et al., 1996). In clinical SCI, daily doses of 300 mg to 4.8 g of GBP have been used safely to treat neuropathic pain and spasticity (Fenollosa et al., 1993; Hagen and Rekand, 2015; Levendoglu et al., 2004; Putzke et al., 2002; Tai et al., 2002; To et al., 2002; Yang et al., 2013). Recent data indicate that GBP and a similar gabapentanoid, pregabalin, when given within the first month post-injury, may also improve motor function in individuals with SCI (Warner et al., 2017). In experimental models of SCI, acute low-dose (50 mg/kg) GBP limits AD severity in rats (Rabchevsky et al., 2010, 2011), and GBP and pregabalin promote axonal regeneration in SCI mice (Sun et al., 2020; Tedeschi et al., 2016). It is unknown whether GBP, when delivered early post-injury as a prophylactic therapy and at human-equivalent doses, will block excitatory synaptogenesis in the spinal cord and provide long-term protection from dysautonomia.

Here we show that high-dose GBP treatment, starting 1 day post-injury (dpi), prevents excitatory synaptogenesis, sprouting of sympathetic neurons that innervate lymphoid tissue, and sprouting of nociceptive afferents in mice with T3 SCI. GBP-dependent inhibition of structural plasticity is associated with reduced frequency of spontaneous AD, reduced severity of induced AD, and protection from immune suppression. These therapeutic benefits persist for up to 1 month after stopping GBP treatment. Reduction of multivariate data to principal components reveals that structural and functional indices of dysautonomia predict a “spinal sympathetic reflex index” and the therapeutic benefit of prophylactic GBP (pGBP). The dose of GBP used in these studies (200 mg/kg/day) is a human-equivalent dose of ~1.1 g daily, well within the dose range used clinically (Nair and Jacob, 2016). Thus, GBP should not only be thought of as a drug to alleviate neurological symptoms after

they develop. Rather, GBP can be an effective prophylactic therapy to prevent maladaptive structural plasticity and pathological dysautonomia caused by high-level SCI and other neurological disorders.

RESULTS

Synaptic plasticity and excitatory synaptogenesis increase progressively in spinal autonomic circuitry after SCI

To determine the extent and timing of synaptic remodeling in sympathetic circuits after SCI, spatiotemporal changes of the excitatory presynaptic marker VGlut2 were quantified in the intermediolateral cell column (IML) at each spinal level between T5–T10. Before injury, the IML contained 190 ± 19 VGlut2$^+$ puncta/160 μm^2. This number decreased ~40% at 3 dpi (115 ± 5 puncta/160 μm^2, p = 0.0075). However, this acute post-injury reduction was transient; the average number of VGlut2$^+$ puncta increased progressively 1.4-fold over baseline levels by 14 dpi (267 ± 14 puncta/160 μm^2, p = 0.0109), 1.6-fold at 21 dpi (311 ± 25 puncta/160 μm^2, p = 0.0001), and more than 2-fold by 28 dpi (389 ± 24 puncta/160 μm^2, p < 0.0001) (Figures S1A and S1B). A detailed analysis of individual spinal levels revealed that the most robust increase occurred at spinal levels T7–T9, where numbers of synaptic puncta increased up to 2.8-fold over baseline between 14–28 dpi (Figures S1B–S1H). The delayed and progressive increase in VGlut2$^+$ puncta in chronic SCI coincided with an increase in expression of α2δ−1 on neurons within the IML; VGlut2$^+$ puncta and the number of α2δ−1$^+$ neurons decreased transiently at 3 dpi and then increased between 3–28 dpi (Figure S2). Gene and protein levels of TSP4, the ligand for α2δ−1, also increased in chronic SCI compared with sham levels (Figure S3).

Next, in an independent experiment, we expanded the scope of our analysis to determine whether high-level SCI causes an increase in functional excitatory synapses in the IML after chronic (35 dpi) SCI. To do this, we combined VGlut2, a presynaptic marker, with the postsynaptic marker Homer1 and then quantified regions where these markers spatially overlapped to form functional synapses. Consistent with the data in Figure S1, the number of excitatory synapses in spinal autonomic regions below the level of injury increased markedly in SCI + saline mice relative to sham-operated saline control mice (Figures 1A and 1B). Higher variation in synapse numbers was observed at spinal levels closer to the injury site (data not shown), but caudal to the lesion, a consistent increase in synaptic density was noted across T5–T10 (sham + saline = 45.79 ± 10.14/160 μm^2, SCI + saline = 78.05 ± 7.39/160 μm^2, p = 0.0408; Figure 1B).

Acute post-injury treatment with GBP blocks excitatory synaptogenesis in spinal autonomic nuclei after SCI

Because GBP blocks α2δ−1-mediated synaptogenesis in the brain (Eroglu et al., 2009), we tested the hypothesis that acute post-injury administration of GBP, starting before onset of enhanced synaptogenesis (Figure S1), would inhibit the SCI-induced increase in excitatory synaptic density. The optimal GBP dose is 200 mg/kg, delivered via 3 daily subcutaneous injections of 66.7 mg/kg GBP every 8 h beginning at 1 dpi through 5 weeks post-injury (Figure S4; STAR methods). In SCI mice treated with this pGBP regimen, the number of

synapses was no different in than sham-operated mice treated with saline (SCI + GBP = 44.13 ± 6.91, sham + saline = 45.79 ± 10.14, p = 0.99; Figure 1B). pGBP injections did not affect synapse number in sham-operated mice (sham + GBP = 43.95 ± 4.93, sham + saline = 45.79 ± 10.14, p = 0.89; Figures S5A and S5B). These data show that high-level SCI causes prolific expansion of excitatory synapses within regions of the spinal cord that control sympathetic drive to the periphery and that pGBP prevents this synaptic plasticity.

pGBP blocks plasticity of sympathetic neurons that control the spleen

We next investigated whether pGBP inhibits aberrant sprouting of SPNs and relevant interneurons that control sympathetic innervation of the spleen, a major immune organ important for controlling host defense. To do this, a GFP-tagged pseudorabies virus (PRV-GFP) was injected into the spleen of SCI mice treated with pGBP or saline (Cano et al., 2001; Ueno et al., 2016). Previously, we and others proved that, in the intact spinal cord of mice and rats, retrogradely labeled PRV-GFP$^+$ neurons are found exclusively in SPNs ipsilateral to the intrasplenic injection, mostly within the lateral and intermediate gray matter from T4–T9 (Cano et al., 2001; Ueno et al., 2016). However, consistent with our previous data (Ueno et al., 2016), after high-level SCI, many more PRV-GFP$^+$ neurons are found throughout the lateral, intermediate, and medial zones of thoracic spinal cord gray matter ipsi- and contralateral to the injection site (Figure 1C). Many GFP$^+$ neurons in the medial and intermediate zones after T3 SCI are excitatory interneurons that form new synapses with SPNs (Ueno et al., 2016). Remarkably, the number of PRV-GFP$^+$ neurons in ipsilateral gray matter was reduced more than 50% by pGBP (Figure 1D). A much larger therapeutic effect was observed in the contralateral spinal gray matter, where the number of PRV-GFP$^+$ neurons decreased 3-fold in GBP-treated mice compared with mice treated with saline (Figure 1E). These data indicate that pGBP blocks aberrant structural plasticity in denervated spinal segments and prevents SCI-induced expansion of sympathetic networks that control the immune system.

Maladaptive sprouting of sensory afferents is blocked by pGBP

Because GBP prevented excitatory synaptogenesis and sprouting of spleen-associated autonomic circuitry below the level of the SCI, we hypothesized that it may similarly affect calcitonin gene-related peptide (CGRP)$^+$ sensory afferent fibers in the lumbar spinal cord that promote pain and AD in animals and humans with SCI (Ackery et al., 2007; Krenz and Weaver, 1998; McNeill et al., 1990; Weaver et al., 2001; Zinck et al., 2007). Examination of CGRP$^+$ immunoreactive profiles in the lumbar (L4 spinal level) dorsal horn revealed that SCI increased the proportional area of CGRP$^+$ fibers in laminae I–II by 1.2-fold (p = 0.022; Figures 2A, 2B, and 2D) and in laminae III–V by 1.5-fold over sham levels (p = 0.027; Figures 2A, 2B, and 2E). SCI also increased the overall length of CGRP$^+$ axons. In contrast to sham-operated (control) mice, where most CGRP$^+$ axons were typically less than 0.3 mm long and rarely extended beyond lamina III in the spinal cord dorsal horn (Figures 2F and 2G), after SCI, CGRP$^+$ axons extended deeper into the gray matter, with 7 of 8 mice having longest axons of more than 0.3 mm and 4 of 8 mice having longest axons of more than 0.4 mm. In SCI mice treated with pGBP, CGRP sprouting did not occur (Figures 2C–2E). As a result, there was a significant reduction in the proportional area of CGRP$^+$ axons in laminae I–II (p = 0.0079) and laminae III–V (p = 0.030) in the SCI + GBP group versus the SCI +

saline group. In fact, pGBP normalized the length of the longest axon to sham levels, with 1 of 8 mice having a longest axon of more than 0.3 mm. On average, SCI increased the length of the longest axon by 0.15 mm (1.6-fold increase over sham, $p = 0.0004$), but SCI + GBP mice did not display this phenotype (−0.01 mm difference compared with sham, $p = 0.99$) and had significantly less axon elongation compared with SCI + saline control mice (1.7-fold reduction, $p = 0.0002$) (Figures 2F and 2G).

Although $CGRP^+$ afferents are normally restricted to superficial Rexed laminae, some are located in the dorsal gray commissure and decussate around the central canal (lamina X), interspersed with autonomic neurons that control the pelvic viscera. This region is thought to be a hub for nociceptive and visceral sensory information that is then relayed rostrally, including to SPNs (Hou et al., 2008; Matsushita, 1998). High-level SCI increased the density of $CGRP^+$ fibers in lamina X by 2.6-fold over sham levels (Figures 2H–2K). This phenotype was eliminated by pGBP ($p = 0.015$ versus SCI + saline, $p = 0.99$ versus sham + saline). When sham-operated control mice received pGBP, neither $CGRP^+$ axon density nor axon length were changed (in any lamina) compared with sham-operated mice treated with saline (sham + GBP versus sham + saline; laminae I–II, $p = 0.59$; laminae III–V, $p = 0.71$; lamina X, $p = 0.12$; longest axon, $p = 0.36$; Figures S5D–5F). These data indicate that pGBP inhibits SCI-induced branching and elongation of lumbar $CGRP^+$ fibers but does not affect pre-existing (intact) autonomic/nociceptive circuitry.

pGBP prevents hyper-excitability of neurons below the level of injury

Next we used FosB immunostaining to determine whether the enhanced structural plasticity that develops below the level of injury is associated with increased neuronal activity within the affected circuitry. Compared with sham + saline control mice, baseline neuronal activity in laminae I–IV was unaffected by SCI, regardless of whether mice were treated with saline or pGBP (Figures 3A and 3B). Conversely, in laminae V–X, where SPNs and excitatory interneurons and increased numbers of $CGRP^+$ axons reside, the number of $FosB^+$ neurons increased ~3-fold in SCI mice (SCI + saline versus sham + saline, $p < 0.0001$; Figure 3C). In SCI mice treated with pGBP, neuronal activation in laminae V–X was reduced ~2-fold compared with SCI + saline mice ($p = 0.036$; Figures 3A and 3C). In fact, neuronal excitability in GBP-treated SCI mice was not different from that of uninjured control (sham + saline) mice ($p = 0.29$). These data indicate that pGBP prevents an increase in neuronal activity in intermediate gray matter, presumably because of the blockade of structural remodeling in excitatory autonomic circuitry.

pGBP delays onset and reduces the frequency of spontaneous AD

Because GBP prevented structural plasticity with a concomitant decrease in sympathetic neuronal activity after SCI, we predicted that development of spontaneous AD would also be reduced. To test this hypothesis, *in vivo* telemetry was used to continuously measure heart rate and blood pressure for up to 30 dpi in T3 SCI mice treated with saline or GBP (Mayorov et al., 2001; Rabchevsky et al., 2012; Zhang et al., 2013). Spontaneous episodes of AD were quantified using a custom algorithm (STAR methods).

Although spontaneous AD was detected in all T3 SCI mice, regardless of treatment, AD frequency was reduced by pGBP. Consistent with previously published data from our lab (Zhang et al., 2013), SCI control mice (SCI + saline) exhibited an initial wave of spontaneous AD (phase I) between 7–12 dpi, with mice experiencing ~7–10 AD events/day. A second phase of AD developed at ~15 dpi (8 events/day), increasing in frequency until ~30 dpi (10–17 events/day) (Figure 4A). Strikingly, pGBP essentially eliminated phase I AD; SCI mice experienced ~3–5 AD events/day from 4–21 dpi. Phase II AD was also less severe, with GBP-treated mice experiencing ~5–10 AD events/day from 21–30 dpi (Figure 4A). The rate of increase in AD events was decreased significantly as a result of pGBP ($p = 0.0153$, mixed effects model). The percentage of mice that experienced high-frequency AD (>8 events per day; STAR methods) was reduced significantly by pGBP. Specifically, 50% of mice (7 of 14) in the SCI + saline group experienced more than 8 AD events per day (mean frequency = 10 events/day) compared with only 19% of mice (3 of 16) in the SCI + GBP group that experienced more than 8 AD events per day (mean frequency = 6 events/day, $p < 0.0001$) (Figure 4B). Moreover, the maximum number of daily AD events experienced during chronic SCI correlated significantly with the number of PRV^+ spinal autonomic neurons (Figures S6A–S6C) and sprouting of $CGRP^+$ primary afferents in the lumbar spinal cord (Figures S6D–S6F). Although AD frequency was decreased by pGBP, the severity and duration of each AD event, as measured by concomitant hypertension with bradycardia, were unaffected. The ability of pGBP to decrease episodic AD was verified in two independent experiments.

The ability of pGBP to inhibit post-injury synaptogenesis in autonomic circuitry likely accounts for the reduction in spontaneous AD. If true, then enhancing synaptogenic function by overexpressing α2δ−1 should increase AD frequency beyond what occurs normally after SCI. To test this hypothesis, we measured the development of spontaneous AD in α2δ−1 transgenic mice (“gain of function”). Littermate control mice (α2δ−1 wild type [WT] on a 129SVE background) developed modest spontaneous AD, experiencing 3–7 events/day from 20–30 dpi (Figure 4C). Differences in the rate and frequency of AD between control groups in Figure 4A and Figure 4C are likely explained by genetic variations in the background strains (Brown and Jacob, 2006; Jacob et al., 2003; Kigerl et al., 2006). Nonetheless, transgenic overexpression of neuronal α2δ−1 (α2δ−1 TG) significantly increased AD frequency compared with α2δ−1 WT littermate controls. After SCI, the α2δ−1 TG group experienced 7–36 events/day (Figures 4C and 4D). Considered together, the data in Figures 1, 2, 3, and 4A–4D indicate that post-injury activation of neuronal α2δ−1 increases structural plasticity with a corresponding increase in the frequency of spontaneous AD.

As an additional level of proof that pGBP treatment reduces AD by blocking maladaptive plasticity within spinal autonomic circuitry, we used colorectal distention (CRD) or cutaneous pinch (CP) stimuli to intentionally elicit visceral or somatic activation of sympathetic reflexes, respectively. Each stimulus was applied individually to SCI mice treated with saline (control) or pGBP. In SCI control mice, CRD elicited consistent AD marked by increased arterial blood pressure of ~20 millimeters of mercury (mmHg) ($p = 0.0019$) with a concomitant drop in heart rate of ~80 beats per minute (BPM) ($p = 0.0225$) (Figures 4E and 4G). AD was elicited similarly by CP, with blood pressure increasing ~20 mmHg ($p = 0.0007$) with a decrease in heart rate of ~130 BPM ($p = 0.0011$) (Figures 4H

and 4J). The same stimuli, when applied to SCI mice treated with pGBP, did not consistently elicit AD; neither CRD nor CP caused hypertension with concurrent bradycardia (Figures 4F, 4G, 4I, and 4J). In fact, in pGBP-treated mice, CRD and CP irritated the mice and caused the heart rate to increase in most mice. These data indicate that the ability of pGBP to block aberrant synaptogenesis and structural plasticity after SCI can reduce pathological cardiovascular reflexes and inhibit the frequency of AD.

SCI-induced immune suppression is prevented by pGBP

Previously we proved, in SCI humans and mice, that activating spinal sympathetic reflexes that trigger AD causes systemic immune suppression (Zhang et al., 2013). Because pGBP reduced AD and associated structural plasticity in the injured spinal cord, we tested the hypothesis that it could also prevent post-injury immune suppression. Consistent with previous data from our group and others (Lucin et al., 2007; Mironets et al., 2018; Prüss et al., 2017; Ueno et al., 2016), T3 SCI caused marked splenic atrophy; spleen weight decreased ~25% relative to sham controls ($p = 0.032$) at 35 dpi (Figures 5A and 5B). pGBP blocked splenic atrophy; spleens from mice treated with pGBP were significantly larger than spleens from SCI control (saline) mice ($p = 0.022$; Figures 5A and 5B).

In SCI + saline mice, splenic atrophy was associated with a 38% reduction of $B220^+$ B lymphocytes ($p = 0.020$) and a 45% reduction of $CD3^+$ T lymphocytes ($p = 0.029$) (Figures 5C, 5D, 5F, and 5G) compared with sham + saline control mice. SCI-induced splenic lymphopenia was prevented by pGBP; white pulp B and T lymphocyte numbers were maintained at control levels (SCI + GBP versus SCI + saline, $p = 0.0053$ for B cell area, $p = 0.048$ for T cell area; SCI + GBP versus sham + saline, $p = 1.99$ for B cell area, $p = 0.99$ for T cell area; Figures 5C–5G). These data show that, by eliminating aberrant spinal autonomic and sensory nerve plasticity, pGBP also blocks onset of post-SCI immune suppression.

pGBP can reduce maladaptive synaptic plasticity long after stopping treatment

In a separate cohort of mice, we determined whether the ability of pGBP to inhibit intraspinal reorganization persists into chronic stages of recovery, even 14 or 28 days after stopping GBP treatment (i.e., 42 or 56 dpi). As in Figure 1, SCI mice treated with pGBP from 1–28 dpi and sacrificed at 28 dpi (no drug withdrawal) had fewer excitatory synapses in the thoracic (T6–T9) IML compared with SCI mice treated with saline (Figures 6A and 6D and quantified in 6H; $p = 0.0385$). An effect of pGBP was still evident 14 (42 dpi) and 28 days (56 dpi) after stopping treatment. Although two potential “non-responders” thwarted statistically significant effects in the 14 day withdrawal group (Figures 6B and 6E and quantified in 6H; $p = 0.4748$), mice in the 28 day withdrawal group had significantly fewer excitatory synapses compared with mice given saline (Figures 6C and 6F and quantified in 6H; $p = 0.0132$).

In SCI + saline mice, the number of excitatory synapses did not increase significantly between 28–56 dpi (Figure 6H), indicating that the mechanisms regulating excitatory synaptogenesis in the SCI mouse are most active during the first 4 weeks post-SCI. Because the number of $\alpha 2\delta{-}1^+$ neurons also increased during this critical period (Figure S2), and

increasing α2δ−1 expression is proposed as a mechanism driving excitatory synaptogenesis (Christopherson et al., 2005), we asked whether the prolonged reduction in synaptogenesis in GBP-treated mice, even after drug withdrawal, was accompanied by a corresponding reduction in α2δ−1 expression. Consistent with the data in Figure S2, after SCI, α2δ−1 expression increased above baseline (sham-operated) levels in the T7 IML at 28, 42, and 56 dpi (Figure S7), with peak levels achieved at 28 dpi. This post-injury induction of α2δ−1 was blocked by pGBP. In mice treated with pGBP, α2δ−1 expression was reduced significantly relative to saline-treated mice, and these treatment effects persisted at even after 14 or 28 d of treatment washout (42 and 56 dpi, respectively) (Figure S7). These data suggest that the ability of GBP to reduce excitatory synaptogenesis, even after drug withdrawal, is linked to GBP-mediated reduction of neuronal α2δ−1 expression.

pGBP inhibits SCI-induced sprouting of lumbar CGRP$^+$ sensory axons long after stopping treatment

To determine whether pGBP has lasting effects on blocking sprouting of CGRP$^+$ primary afferent fibers (Figure 2), we next quantified the area and length of CGRP$^+$ axons throughout spinal gray matter laminae in the lumbar dorsal horn using spinal cords from the same mice that were used in Figures 6A–6H to quantify excitatory synapses. Within-group comparisons revealed that, among control SCI mice (saline treatment 1–28 dpi; Figures 6I–6K), the area of CGRP$^+$ axons did not increase significantly between 4–8 weeks post-SCI within laminae I–II ($p = 0.99$; Figure 6O) or laminae III–V ($p = 0.064$; Figure 6P). However, in lamina X, the CGRP$^+$ area increased significantly as a function of time post-injury ($p = 0.017$; Figure 6Q), as did the length of the longest CGRP$^+$ axon ($p = 0.0019$; Figure 6R). A time-dependent increase in the area occupied by CGRP$^+$ axons was also noted in SCI mice treated with pGBP (SCI + GBP; Figures 6L–6N), but only in laminae I–II ($p = 0.038$, 4 versus 6 weeks; $p = 0.025$, 4 versus 8 weeks; Figure 6O). Also, at 8 weeks post-injury in GBP-treated mice, the length of the longest CGRP$^+$ axon increased relative to axons at 4 weeks post-injury ($p = 0.0045$ versus 4 weeks; Figure 6R).

Between-group comparisons (saline versus GBP) at matched post-injury time points revealed a significant effect of pGBP on reducing CGRP sprouting and axon growth up to 1 month after stopping GBP treatment. These therapeutic effects were evident in all gray matter laminae but were consistently robust in deeper laminae. Specifically, as shown in Figure 2, pGBP reduced the area and maximum length of CGRP$^+$ axons in all spinal gray matter laminae compared with saline-treated counterparts (laminae I–II, 1.5-fold reduction, $p = 0.018$; laminae III–V, 2.3-fold reduction, $p = 0.047$; lamina X, 2.5-fold reduction, $p = 0.049$; longest axon = 1.6-fold reduction; $p = 0.0036$; Figures 6O–6R). The magnitude of afferent CGRP$^+$ fiber sprouting, although not significantly different from saline controls, was still reduced by pGBP in the superficial and deep spinal laminae of most SCI mice even 14 (42 dpi) or 28 days (56 dpi) after treatment was stopped (14 d withdrawal: laminae I–II, 1.2-fold reduction, $p = 0.11$; laminae III–V, 1.7-fold reduction, $p = 0.095$, 28 d withdrawal: laminae I–II, 1.2-fold reduction, $p = 0.058$; laminae III–V, 1.7-fold reduction, $p = 0.1$; Figures 6O and 6P). In spinal lamina X, pGBP significantly reduced CGRP$^+$ fiber sprouting 14 (1.9-fold reduction, $p = 0.014$; Figure 6Q) and 28 days after GBP withdrawal (2-fold reduction, $p = 0.0004$; Figure 6Q). The length of the longest CGRP$^+$ axon was also reduced

in both GBP withdrawal groups relative to time-matched SCI saline controls (1.4-fold reduction at 42 dpi,$p = 0.025$; and 56 dpi,$p = 0.014$; Figure 6R). These data indicate that severe high-level SCI causes $CGRP^+$ axons continue to sprout and then grow longer axons that penetrate into deeper layers of lumbar spinal cord gray matter for at least 8 weeks after injury. This time-dependent increase in sprouting and elongation of $CGRP^+$ lumbar sensory axons can be prevented by pGBP, even up to 4 weeks after stopping GBP treatment.

Lasting blockade of maladaptive plasticity by pGBP also reduces pathological dysautonomia

To determine whether the lasting protection conferred by pGBP against maladaptive plasticity extends to functional measures of dysautonomia, we used techniques identical to those shown in Figure 5 to measure surrogates of systemic immune function in mice shown in Figure 6. We show that loss of T and B lymphocytes is blocked by pGBP even 4 weeks after treatment withdrawal (Figures S8A–S8H).

Although we could not measure AD in the same mice used to evaluate the effects of GBP withdrawal, independent studies have confirmed a direct correlation between the magnitude of $CGRP^+$ sprouting in the lumbar spinal cord and the frequency or severity of AD (Cameron et al., 2006; Krenz et al., 1999; Weaver et al., 2001; Figure S6). We show that structure-function correlations also exist between indices of immune suppression and structural measures of autonomic plasticity. Specifically, the number of excitatory synapses and measures of CGRP plasticity are inversely correlated with splenic lymphocyte numbers (Figures S8I–S8M). These correlations also reveal a robust effect of pGBP (note the clear separation between treatment groups).

To extend these individual bivariate correlations, we applied syndromic analyses. Syndromics is a multivariate statistical framework for integrating various neurotrauma data with the goal of revealing potential associations among diverse injury- and treatment-dependent structural and functional outcome measures (Ferguson et al., 2011). Multivariate approaches are sensitive to associations among multiple outcomes and can identify underlying disease states that are unconstrained by the limitations of individual measures. In SCI modeling, multivariate pattern detectors, such as principal-component analysis (PCA), have been used to distill numerous variable outcome measures down to a few multivariate patterns or principal components (PCs). Because, in this study, several measures of structural change (e.g., $\alpha 2\delta{-}1$ expression, excitatory synapses, $CGRP^+$ axon sprouting, and PRV^+ neuron tracing) and functional dysautonomia (e.g., splenic lymphocyte numbers, spleen weight, and AD) were analyzed simultaneously in individual mice, we performed two PCA experiments. Experiment 1 (Figures 7A, 7C, and 7E) returned 7 PCs (PC1–PC7), and experiment 2 (Figures 7B, 7D, and 7F) returned 8 PCs (PC1–PC8), with decreasing contributions to the overall variance. In both experiments, PC1 captured most of the variance: 65.9% in experiment 1 (Figures 7A and 7C) and 50.6% in experiment 2 (Figures 7B and 7D). PC2 accounted for only 14.6% and 15.1% of the variance in experiments 1 and 2, respectively; other PCs accounted for 0.1%–10.2% of the variance. PC1, the major PC, was loaded negatively by CGRP, PRV^+ neurons, AD, excitatory synapses, and $\alpha 2\delta{-}1$ expression and loaded positively by splenic atrophy and B and T lymphocyte loss

(Figures 7A and 7B). Because PC1 accounted for most of the variance between mice across a collection of structural and functional outcome measures, PC1 was designated the "spinal sympathetic reflex index." In both PCA experiments, SCI + saline mice were shifted negatively on the spinal sympathetic reflex index (PC1), and SCI + GBP mice were shifted positivity on the spinal sympathetic reflex index (PC1) (Figures 7C and 7D).

Next we collected PC1 scores from individual mice to test the hypothesis that the spinal sympathetic reflex index was significantly different between the SCI + saline and SCI + GBP groups. Analysis of mice in PCA experiment 1 revealed that SCI + saline mice had a significantly lower (more impaired) spinal sympathetic reflex index compared with SCI + GBP mice (SCI + saline = −1.0 ± 0.58, SCI + GBP = 0.88 ± 0.44, $p = 0.014$; Figure 7E). PCA experiment 2, which included SCI mice at 28 dpi (no treatment withdrawal), 35 dpi (no treatment withdrawal), 42 dpi (14 d treatment withdrawal) or 56 dpi (28 d treatment withdrawal), similarly revealed a significant separation between the saline and GBP groups ($p < 0.0001$) and also a significant effect of time post-SCI ($p < 0.0001$) (Figure 7F). Post hoc analysis showed that the saline and GBP groups were significantly different at all time points ($p < 0.0001$; Figure 7F). These syndromic analyses show that the structural and functional readouts of dysautonomia used in the current study can predict treatment effects on the spinal sympathetic reflex even up to 4 weeks after stopping treatment.

DISCUSSION

GBP is a first-line treatment for established neuropathic pain after SCI (Levendoglu et al., 2004; To et al., 2002). The data in this report show that GBP could also be considered for use as a prophylactic therapy, with treatment beginning early after SCI. Indeed, in mice with severe T3 SCI, pGBP prevents excitatory synapse formation on SPNs and surrounding interneurons, sprouting of spinal-splenic interneurons, and branching of visceral/nociceptive afferents. pGBP also prevents SCI mice from developing AD and immune suppression, two secondary complications of dysautonomia that impair quality of life for individuals with SCI (Anderson, 2004; Failli et al., 2012; Prüss et al., 2017; Zhang et al., 2013). The therapeutic benefits of pGBP are evident even 1 month after stopping treatment.

pGBP inhibits maladaptive plasticity after SCI

Anatomical reorganization of autonomic circuitry caudal to the lesion occurs in three stages in SCI mice. The first two stages, described previously in a rat SCI model using electron microscopy, are marked by loss of axo-somatic and axo-dendritic glutamatergic inputs to SPNs below the injury at 3 dpi (stage 1) with partial recovery of synapse numbers by 14 dpi (stage 2) (Krassioukov and Weaver, 1995; Llewellyn-Smith and Weaver, 2001; Llewellyn-Smith et al., 2006). Stage 1 is likely caused by rapid deafferentation of interneurons and SPNs because of loss of descending bulbospinal and propriospinal axons (Ditunno et al., 2004; Jansen et al., 1995; Zagon and Smith, 1993). Stage 2 coincides with enhanced growth-associated protein expression in axon terminals that synapse on SPNs (Weaver et al., 1997). Extending these data, we show that post-SCI changes in excitatory inputs occur throughout the IML and continue throughout a third and protracted stage 3 (>14 dpi) when supernumerary excitatory synapses occupy previously vacant synaptic sites and also

SPN soma. This plasticity is robust at spinal levels T6–T9, which, at a minimum, supply sympathetic output to the adrenal gland, spleen, liver, kidney, and splanchnic vasculature. Our analysis of α2δ−1 expression, combined with other data (Bikbaev et al., 2020; Eroglu et al., 2009), implicate α2δ−1 calcium channel subunits in development of these expanded excitatory neuronal networks.

α2δ−1 promotes pre- and post-synaptic protein assembly. TSPs produced by astrocytes and microglia bind to α2δ−1 subunits on neurons, activating Rac1 and the synaptogenic signaling complex (Christopherson et al., 2005; Eroglu et al., 2009; Risher et al., 2018). Intraspinal TSPs increase within 12 h and remain elevated weeks after SCI (Boroujerdi et al., 2011; Wang et al., 2009; Zeng et al., 2013), a finding reproduced here. Our data also show that α2δ−1 expression increases progressively over time, corresponding with a period of protracted synaptogenesis (stage 3). A recent study discovered that α2δ−1 per se increases excitatory synaptic density and network connectivity during neural development (Bikbaev et al., 2020). Sustained post-injury elevations in TSP and α2δ−1 would therefore create an environment that favors formation and stabilization of new synapses on SPNs and other neurons projecting to them. By keeping α2δ−1 in an inactive conformation, pGBP likely blocks TSP- and α2δ−1-dependent synaptogenesis and subsequent increases in neuronal excitability (Eroglu et al., 2009; Risher and Eroglu, 2012; Risher et al., 2018). GBP-mediated inhibition of synaptogenesis would also explain why structural remodeling of spinal-splenic circuits, as defined by PRV labeling, was reduced.

Because GBP blocks α2δ−1 synaptogenic signaling, it also inhibits excitatory neurotransmission and likely production of neurotrophic factors. α2δ−1 facilitates neuronal activity by increasing calcium transients, increasing pre-synaptic glutamate release, and trafficking of calcium channels and *N*-methyl-D-aspartate (NMDA) glutamate receptors to the cell surface; each is blocked by GBP (Bauer et al., 2009; Chen et al., 2018; Field et al., 2006; Hendrich et al., 2008). Using FosB as a marker of neuronal activity (Malik et al., 2014), we show that the excitability of spinal autonomic neuronal networks increases after SCI. Accumulation of FosB increases brain-derived neurotrophic factor (BDNF) production, which increases dendritic branches and spines on neurons (Kellner et al., 2014). FosB levels in GBP-treated SCI mice were close to sham levels, suggesting that inhibition of activity-dependent plasticity may partly explain why pGBP reduces post-injury synaptic plasticity. However, long-term blockade of structural remodeling, rather than inhibition of excitatory activity, would better explain why, even a month after treatment withdrawal, pGBP reduces synapse numbers in the thoracic IML and indices of functional dysautonomia, as revealed by blockade of post-SCI immune suppression. Regardless of the mechanism by which α2δ−1 promotes structural remodeling, the functional consequences of increasing α2δ−1 expression are evident not only from GBP-mediated blockade but also by the genetic gain-of-function study showing that AD frequency after SCI is exacerbated by TG overexpression of neuronal α2δ−1. α2δ−1 TG mice are on a different genetic background (129SV) than the C57BL/6J mice used to test the effects of pGBP on reducing AD. Genetic differences are key variables that influence SCI pathology and dysautonomia after SCI (Brown and Jacob, 2006; Jacob et al., 2003; Kigerl et al., 2006), so control group data between the different experiments should not be compared directly. The potential for animal strain/species to influence autonomic data after SCI is also highlighted by a study showing that continuous

GBP (400 mg/kg/day) increases daily AD events in Wistar rats with T4 transection SCI (Eldahan et al., 2020), although control rats had few events in that study.

Non-synaptic effects of GBP

Because α2δ−1 expression is not limited to neurons, we cannot discount the possibility that benefits of pGBP occur through other α2δ−1-dependent but synapse-independent effects. For example, below the level of injury, activated spinal cord glia increase expression of tumor necrosis factor (TNF), which promotes afferent sprouting and exacerbates AD and neuropathic pain (Mironets et al., 2018). GBP inhibits production of TNF (Lee et al., 2013), suggesting that GBP-dependent inhibition of axonal sprouting and synaptogenesis could be explained partly by reduction of neuroinflammatory signaling in the spinal parenchyma.

GBP and gabapentinoids (e.g., pregabalin) target voltage-gated calcium channels, but there are differences in the α2δ calcium channel subunits they target. GBP has a higher affinity for the α2δ−1 subunit, whereas pregabalin is more specific for α2δ−2 (Gong et al., 2001). These proteins, as well as α2δ−3 and α2δ−4, have distinct patterns of expression throughout the body (Cole et al., 2005; Gong et al., 2001). Notably, outside of the CNS, α2δ−1 is expressed in cardiac tissue, smooth muscle, and endocrine organs (Dolphin, 2013), so we cannot rule out the possibility that systemic pGBP blocked dysautonomia by acting directly on peripheral tissues. In comparison, α2δ−2 is predominantly expressed in the CNS (Dolphin, 2013). α2δ−2 has been identified recently as a developmental switch that inhibits CNS axon growth (Tedeschi et al., 2016), and dorsal root ganglion (DRG) neurons from mice treated with pregabalin show stronger intrinsic growth potential *ex vivo* than naive DRG neurons. Moreover, systemic pregabalin promotes axon regeneration after SCI (Tedeschi et al., 2016). These differences in α2δ subunit binding affinity of gabapentinoids and tissue distribution of α2δ subunits could explain why axon outgrowth is blocked by GBP but enhanced by pregabalin (Cole et al., 2005; Tedeschi et al., 2016). Intriguingly, systemic administration of GBP has been shown recently to increase corticospinal tract outgrowth across the midline following a mouse C5 hemi-section (Sun et al., 2020). Although the precise mechanisms that cause GBP to paradoxically inhibit $CGRP^{+}$ sensory fiber growth while promoting motor tract regeneration are unknown, it is of obvious potential benefit for individuals with SCI if pGBP can do both.

pGBP also inhibits onset of post-injury leukopenia and atrophy in secondary lymphoid tissues. These are immunological surrogates of SCI-induced immune deficiency syndrome (SCI-IDS), a secondary consequence of SCI in humans and animals caused by development of aberrant plasticity in spinal sympathetic circuitry (Ueno et al., 2016; Zhang et al., 2013). SCI-IDS places individuals with SCI at increased risk for developing pneumonia, a leading cause of morbidity and mortality after SCI (Brommer et al., 2016; Kopp et al., 2017; Prüss et al., 2017). It is also possible that pGBP has immunotropic effects through its ability to directly modulate lymphoid tissues and metabolic derangements that normally develop after SCI. Indeed, immune and metabolic processes are inextricably linked, and the α2δ−1 subunit is expressed on various cell types in immune and metabolic organs (Gee et al., 1996; Gong et al., 2001; Hotamisligil, 2017). In this context, if pGBP could protect individuals with SCI from developing infections, it would be a valuable alternative

to antibiotics, which are commonly used in individuals with SCI even though they perturb the microbiome, a disease-modifying factor that can adversely affect neurological recovery and exacerbate systemic physiology after SCI (Kigerl et al., 2016). Furthermore, because individuals with SCI are more susceptible to multi-drug-resistant bacteria (Fitzpatrick et al., 2018), alternatives to antibiotics to fight infection are clearly advantageous.

Dosing and duration of effect of pGBP on post-SCI dysautonomia

Currently, to treat neuropathic pain in individuals with SCI, titrated doses of GBP are started after symptom onset. Doses typically start at 300 mg and increase in 300- to 400-mg increments over 1 week, usually up to 900 mg to 1.8 g/day (Yang et al., 2013). The dose used in our study (200 mg/kg/day) equates to ~1.1 g/day of GBP in humans, which is well within the human dosing range (Hagen and Rekand, 2015; Levendoglu et al., 2004; Nair and Jacob, 2016; To et al., 2002). Our data show that this human-equivalent dose prevents formation of a “supercharged” sympathetic reflex circuit and reduces the frequency of episodic AD in SCI mice. Maintaining high GBP concentrations is likely critical for this outcome because daily administration of low-dose GBP is not sufficient to relieve the frequency of episodic AD (Rabchevsky et al., 2012), even though lower GBP doses, given hours before measurements, are sufficient to reduce the severity of AD, tail spasticity, electromyogram (EMG) activity, and hypersensitivity (Kitzman et al., 2007; Rabchevsky et al., 2011; Tanabe et al., 2009).

When administered acutely after SCI, assuming a need for incremental dosing, it would take ~4–6 days to achieve and sustain the human equivalent dose of 1.1 g/day, which is well before structural plasticity and the systemic consequences of dysautonomia develop. Using different models to extrapolate mouse to human age and time equivalents, it is possible that the benefits of this human-equivalent dose could last 3–11 years in an adult human with SCI (Dutta and Sengupta, 2016; Jackson et al., 2017). Future studies are needed to define optimal treatment duration and dosage, potential interactions with other drugs commonly used in acute post-SCI care, as well as any non-synaptic effects of pGBP that could contribute to drug efficacy or sabotage recovery by exacerbating organ-specific pathology.

In conclusion, acute post-injury treatment with GBP blocks α2δ−1 calcium channel subunits and reduces the maladaptive structural reorganization of spinal sympathetic reflex circuitry that causes pathological dysautonomia. Thus, repurposing GBP as a prophylactic therapy for individuals with high-level SCI may be a feasible, safe, and inexpensive standard of care that, by inhibiting dysautonomia, could improve quality of life and survival after SCI.

STAR★METHODS

RESOURCE AVAILABILITY

Lead contact—Further information and requests for resources and reagents should be directed to and will be fulfilled by the Lead Contact, Phillip. G. Popovich (Phillip.Popovich@osumc.edu).

Materials availability—This study did not generate new unique reagents.

Data and code availability—The datasets generated during this study have been deposited to The Open Data Commons for Spinal Cord Injury (https://doi.org/10.34945/F5V30C).

EXPERIMENTAL MODEL AND SUBJECT DETAILS

Mice—Adult female C57BL/6J mice (n = 183 total) from Jackson Laboratories were used for this study. Mice overexpressing α2δ−1 (α2δ−1 TG, n = 8) and WT littermates (α2δ−1 WT, n = 8), on a 129SVE background also were used (Li et al., 2006). Animals were housed under conventional conditions on a 12 hour light-dark cycle with *ad libitum* access to food and water. Mice were housed in groups of 4 except for the two replicate and transgenic mouse telemetry studies, where individual housing was necessary. Age- and weight-matched mice were used within experiments. In studies comparing the effects of GBP on autonomic dysreflexia (AD) in C57BL/6J mice, two mice from the SCI + saline group died, one as a result of bladder expression complications, and one as the result of anesthetic complications during surgery (Figure 4A). For studies comparing AD in α2δ−1 WT and α2δ−1 TG mice, 4–5 mice per group died after SCI surgery and during the first two weeks of telemetry recording (Figure 4C). The reason for the higher mortality rate in 129SVE mice may have been SCI-induced hypotension in this strain. Specifically, the average BP in the first week after SCI was ~20 mmHg less in α2δ−1 WT and TG mice compared to conventional C57BL/6J mice. In the GBP withdrawal study, 7/54 mice died (2/7 due to autophagy, 5/7 due to suspected respiratory complications; n = 5 GBP and n = 2 saline) (Figure 6). All procedures were performed in accordance with the Ohio State University Institutional Animal Care and Use Committee and the ARRIVE guidelines.

GBP dosing studies—GBP (#PHR1049 Millipore Sigma) was dissolved in saline. We first tested different routes of GBP administration to determine the optimal method to achieve consistent, neuroactive concentrations of GBP within the spinal cord. GBP saturates in pure H2O at 100 mg/ml (Friciu et al., 2017), and we determined it saturates in saline at 133 mg/ml. Therefore, for initial dosing studies we first administered 133 mg/ml GBP via an implanted mini-pump with a delivery rate of 6 μl/day (800 μg total GBP/day or 40 mg/kg), which was the maximum volume possible with the mini-pump. Alternatively, we administered one subcutaneous injection of 133.3 mg/ml GBP to mice (4 mg/30 μL or 200 mg/kg). The injection volume was 5 times higher to account for pharmacokinetic degradation over time at 37°C (Radulovic et al., 1995; Zour et al., 1992). One week after the start of daily GBP injections, mice were sacrificed 2 or 32 h after the last injection. Animals with mini-pumps were sacrificed 1 or 3 weeks after starting mini-pump infusions. Fresh whole spinal cord samples (~100 mg) were homogenized in 0.2 mL of internal standard solution of 100 ppm caffeine in water. Proteins were precipitated with acetonitrile (1.6 mL). The samples were vortexed for 30 s then centrifuged at 13,000 × g for 10 mins at 4°C. The supernatant was transferred to a clean 1.5 mL conical tube and dried completely under a gentle stream of nitrogen gas. Dried samples were stored at −80°C until analysis. High performance liquid chromatography electrospray ionization time-of-flight mass spectrometry was used to quantify the concentration of GBP. Subcutaneous injection yielded the highest concentration of GBP in the spinal cord (Figure S4). The half-life of GBP in the spinal cord was calculated based on the equation (half-life = elapsed time ×

log0.5/log (beginning amount/ending amount) = 30 × log0.5 / log(4195 μg/kg / 35465 μg/kg) = 9.7 hours. Therefore, for all subsequent studies, we selected a GBP dosing regimen of 200 mg/kg/d by administering 66.7 mg/kg GBP three times per day every 8 h for the duration of the experiments.

Treatment groups—Our *a priori* hypothesis was that "prophylactic GBP will prevent the development of structural plasticity within spinal autonomic circuitry after high-level SCI." Although only two experimental groups, i.e., SCI + saline and SCI + GBP, are required to test this hypothesis, two additional control groups were included. Sham + saline mice were included as a negative control to confirm injury-dependent effects on synapse numbers (Figure 1), axon sprouting (Figure 2), neuronal activation (Figure 3), and splenic atrophy (Figure 5), as previously reported by us and others (Cameron et al., 2006; Hou et al., 2008; Krenz et al., 1999; Lucin et al., 2009; Zhang et al., 2013). Sham + GBP mice also were included as a technical control to ensure that GBP did not alter the baseline characteristics of these outcome measures. Since GBP did not affect any outcome measures in uninjured spinal cord (see Figure S5), unless noted otherwise in the results, data in Figures 1B, 2, 3, and 5 compare three groups: the two primary experimental groups (SCI + saline and SCI + GBP) and the negative control group (sham + saline).

Starting the morning after surgery until the final morning of the experiment at 35 days post-sham/SCI, mice were subcutaneously injected with 100 μL of saline or GBP (66.7mg/kg) every 8 hours (3x/day). To ensure that researchers remained blind to treatment group, individuals performing data collection and analyses were only informed of mouse IDs and not the experimental condition.

A separate experiment was performed to determine the duration of effect of GBP after stopping treatment (Figure 6). For this, mice were randomly assigned to receive either saline or GBP (66.7mg/kg) injections every 8 hours (3x/day), and then were randomly assigned to an experimental end point of 28, 42, or 56 days post-injury (dpi). In all groups, treatments began at 1 dpi and continued for 28 dpi. Treatments then stopped and animals were sacrificed at 28, 42, or 56 dpi, corresponding with 0, 14, or 28 days after stopping GBP treatment, respectively.

SCI and post-operative care

SCI: Mice were anesthetized by injecting a mixture of ketamine (80 mg/kg) and xylazine (40 mg/kg) into the peritoneum. During surgery, mouse body temperature was maintained at ~37.5°C using a feedback-controlled heating pad (Harvard Apparatus). The third thoracic vertebra (T3) was identified based on anatomical landmarks (i.e., T2 spinous process and supraspinal vasculature). To create a severe, high-level SCI, the spinal cord located between T3 and T4 vertebrae was crushed by inserting Dumont forceps (Fine Science Tools, with tip of 0.4–0.2 mm) 2 mm ventrally into the vertebral column on both sides of the spinal cord, then laterally compressing the spinal cord by bringing the forceps tips together completely, so that they were touching for 3 s. This injury leaves the dura intact but creates a severe lesion with minimal sparing of ascending or descending axons in the white matter (Faulkner et al., 2004). The muscle was sutured with 5.0 polyglactin dissolvable sutures and the skin

closed with wound clips. Sham-operated mice underwent anesthesia and surgical procedures exactly as above but without a spinal crush injury. Completeness of the crush injury was confirmed with end point histology and by visually confirming that complete paralysis of the hind limbs was present at 1 dpi.

Post-operative care: Following surgery, animals were injected with saline (2 ml, s.c.) and antibiotics (Gentocin, 1 mg/kg, s.c.) then placed into warmed cages (~34°C). Bladders from SCI animals were manually voided twice daily for the duration of experiments. Body weight and urinary pH were monitored weekly. To prevent dehydration, mice were supplemented with saline (1–2ml s.c. for 5 dpi). Antibiotic coverage was achieved by administration of gentamicin (1 mg/kg s.c. daily for 5 dpi). Mice showing alkaline urine were presumed to have mild urinary tract infections and were treated with antibiotics until the infection resolved (Baytril, 10 mg/kg s.c.).

METHOD DETAILS

Fluoro-Gold tracing—To retrogradely label all sympathetic preganglionic neurons (SPNs), mice were injected (i.p.) with 100 μL of 1% Fluoro-Gold (Fluorochrome, LLC) 7 days before perfusion (i.e., 21, 28, 35 or 49 days post-spinal surgery) (Schmued and Fallon, 1986). Successful labeling was confirmed by bilateral presence of bright, Fluoro-Gold$^+$ neurons in the thoracic IML and spinal lamina VII.

Tissue processing—At defined experimental end points, mice were anesthetized with 1.5x the surgical dose of ketamine/xylazine (see above) and perfused transcardially with 0.1 M PBS, until blanching of the liver to a light brown color and the perfusate ran clear (~60 s), followed by 4% PFA for 6 mins. Spinal cords were dissected and post-fixed in 4% PFA for 2 h at room temperature, washed in 0.2 M phosphate buffer overnight, then cryopreserved for 48 h in 30% sucrose in 0.1 M PBS. Tissues were embedded in Tissue-Tek optimal cutting temperature compound and stored at −80°C until sectioning. Spinal cords sections were cut along the coronal axis in 1:10 series at 20 μm using a Microm HM 505E Digital Cryostat. Sections were collected onto SuperFrost Plus slides and stored at −20°C until immunostaining.

Immunohistochemistry—For immunofluorescent staining, sections were dried for at least 1 h on a slide warmer, washed in 0.1 M PBS (3 × 4 mins), then blocked for 1 hour in 0.1 M PBS containing 1% bovine serum albumin (BSA) and 0.1% Triton X-100 (BP$^+$). Sections were incubated at 4°C overnight in primary antibody solutions made in BP$^+$ (see Key resources table). After washing in 0.1 M PBS (3 × 4 mins), slides were incubated in fluorophore-conjugated secondary antibodies (see Key resources table) with or without DRAQ5 nuclear dye (1:4000, Abcam, #ab108410) for 1 h at room temperature. Slides underwent a final round of washing before being coverslipped with Immumount media. For α2δ−1 immunostaining, sections underwent heat-induced antigen retrieval (10 mM citrate buffer, pH 6.0, 0.1% Tween 20 at 95°C for 10 mins) before the blocking step.

VGlut2 puncta analysis—Spinal cord sections from sham and SCI mice at 3, 14, 21 and 28 dpi were immunostained for the pre-synaptic protein VGlut2 (Figure S1). Stained

sections were imaged and analyzed using a modified protocol from Ippolito and Eroglu (2010). Briefly, 15-step Z stacks of 0.33 μm increments spanning 5 μm were acquired on an Olympus Filter FV1000 Confocal microscope with 40x magnification and 2x optical zoom (80x final magnification). Imaging parameters were consistent to minimize intensity variability. Z stack steps were compressed serially in groups of three (i.e., steps 1–3, 4–6, 7–9, 11–12, 13–15) to create 5 maximum intensity projections (MIPs). The ImageJ plug-in Puncta Analyzer (written by Bary Wark, available upon request, c.eroglu@cellbio.duke.edu) was used to threshold VGlut2$^+$ signal and count the number of labeled puncta. Details of the method can be found in Ippolito and Eroglu (2010).

Synapse analysis—Each spinal level from T1-T10 was immunostained for the pre- and post-synaptic proteins markers, VGlut2 and Homer1, respectively. Stained sections were imaged and analyzed using a modified protocol from Ippolito and Eroglu (2010). Briefly, 15-step Z stacks of 0.33 μm increments spanning 5 μm were acquired on an Olympus Filter FV1000 Confocal microscope with 40x magnification and 2x optical zoom (80x final magnification). Imaging parameters were consistent to minimize intensity variability. Z stack steps were compressed serially in groups of three (i.e., steps 1–3, 4–6, 7–9, 11–12, 13–15) to create 5 MIPs. Synapse quantification was performed with MIPAR Image Analysis software with a custom semi-automated synapse algorithm (https://www.mipar.us/recipe-store.html). Briefly, the intensity of VGlut2$^+$ and Homer1$^+$ channels was gated based on the median intensity MIP from each image. Puncta > 100 pixels or < 5 pixels were removed from the channel. Puncta in one channel that met these criteria and overlapped spatially with puncta from the other channel were counted as a functional synapse. For representative images (Figures 1 and 6), MIPs of fluorescent images were imported into Adobe Photoshop and a levels adjustment layer was applied to reveal the full tonal range of visible pixels in the RGB histogram.

α2δ−1 expression—Spinal cord sections from sham and SCI mice at 3, 7, 14, 21 and 28 dpi (Figure S2), and from mice in the withdrawal experiment (28, 42 or 56 dpi, treated with saline or GBP from 1–28 dpi) (Figure S7) were immunostained for α2δ−1 and DRAQ5. Stained sections were imaged using 10-step Z stacks of 1 μm increments on a Leica TCS SP8 confocal microscope with 40x magnification. Imaging parameters were consistent to minimize intensity variability. Z stack steps were compressed serially to create one MIP. ImageJ was used to manually count cell bodies and threshold α2δ−1$^+$ staining, which was also expressed as a proportional area of the image.

TSP4 expression

mRNA: Spinal cord tissues (1 cm piece below the lesion, n = 5 for T3 sham and n = 5 for T3 crush, 21 dpi) were homogenized in 1 mL of Trizol reagent (Invitrogen). Total RNA was extracted using Trizol according to the manufacturer's instructions. The total RNA concentration was determined by absorbance at 260/280nm. Reverse transcription was set up using 200 μg total RNA and random primer with iScript Reverse Transcription Supermix (Bio-Rad). Transcripts were quantified using SYBR Green qPCR mastermix and a 7300 Real-time PCR system (Applied Biosystems). Primer sequences used are as follows: mouse TSP4: forward 5′-TGTTTCCGAGGTGTCCGATG-3′;

reverse 5′-GGAGCCAAATTCACACAGCG-3′; mouse 18 s forward: 5′-TTCGGAACTGAGGCCATGAT-3′, reverse: 5′-TTTCGCTCTGGTCCGTCTTG –3′; Fisher Scientific 4319413E). The 18 s gene was used for normalization of TSP4 mRNA concentrations, determined using the ΔCt method (Figure S3)

Protein: T3 sham or T3 crush SCI (21 dpi) (n = 3 mice per group) spinal cord sections (3 sections per mouse at T9) were immunostained for TSP4 and DAPI nuclear dye (Fisher Scientific, #D3571). Stained sections were imaged using on a Leica TCS SP8 confocal microscope with 20x magnification. Imaging parameters were consistent to minimize intensity variability. TSP^+ cells were manually counted, divided by the number of cells in the field of view, and then normalized to sham values (Figure S3).

PRV tracing

Viral delivery: Five days before perfusion (i.e., 30 dpi), the random number generator in Microsoft Excel was used to randomly choose a subset of SCI mice from the SCI + saline and SCI + GBP groups (n = 3 per group). These mice were anesthetized by isoflurane inhalation (2% isoflurane in oxygen during induction and 1.5% for maintenance). The left flank was shaved and sterilized, and a 1 cm diagonal incision was made into the skin and muscle overlying the spleen. The spleen was carefully extracted from the peritoneal cavity and positioned atop sterile gauze placed on the skin. The spleen was injected with a GFP-expressing pseudorabies virus (PRV; Bartha strain PRV152; 4.9 × 109 pfu/ml) using pulled glass pipettes (World Precision Instruments, 1B150F-4) attached to the Nanoject system (World Precision Instruments, PV830 Pneumatic PicoPump) positioned under a dissecting microscope. A total of 10 μL of virus was delivered through 10 injection sites spread evenly along the rostral-caudal axis of the spleen (1 μL per site). Any potential virus leaking from the injection sites was absorbed with a sterile cotton swab. The spleen was then carefully repositioned into the peritoneal cavity. The peritoneal cavity and skin were sutured closed. Mice were placed into warmed cages (34°C) and given 1 cc of saline and antibiotics (Gentocin, 1 mg/kg, s.q.) during anesthesia recovery.

Tissue processing: At 35 dpi, mice were transcardially perfused as described above. Spinal cords were dissected and the T4 and T10 levels were marked *in situ* with a fine permanent marker. These landmarks were used to help define the other spinal levels during image acquisition. Samples were post-fixed in 4% PFA overnight at 4°C then submerged in 0.2 M PB. The thoracic spinal cord was divided into portions (T3-T7 and T8-T12). Horizontal floating sections (80 μm thick) of each thoracic portion were cut on a vibratome (Leica VT1200 S) and slices collected into a 24 well plate containing 0.1 M PBS. Samples were stored at 4°C in the dark until staining and imaging.

IHC and Imaging: Horizontal sections at the depth of the central canal containing GFP^+ neuronal cell bodies (i.e., the IML cell column) were transferred to a 96 well plate. Sections were blocked in BP^+ for 2 hr, then incubated with Chicken anti-GFP (1:500; Aves) for 72 hours at 4°C. After washing with 0.1% Triton X-100 in PBS, sections were incubated with goat anti-chicken Alexa Fluor 488 (Invitrogen A-11039) for 72 hours. After washing, sections were mounted with VECTASHIELD antifade mounting medium (Vector, H-1000)

on ColorFrost slides (Cat. # 9951L-006). To visualize the splenic neuronal network in the thoracic spinal cord, 10-step Z stacks of 8 μm increments spanning 80 μm were acquired using a Leica TCS SP8 confocal microscope with 10 X magnification. High-resolution images of the entire horizontal section were created using tiling with automatic stitching. MIPs of representative fluorescent images (Figures 1C and 1D) were imported into Adobe Photoshop and a levels adjustment layer was applied to reveal the full tonal range of visible pixels in the RGB histogram.

Quantification of PRV$^+$ neurons: The thoracic gray matter was divided into the ipsilateral (left) and contralateral (right) sides relative to the location of the spleen. Each side was then sub-divided into the medial zone where the central autonomic nucleus is located (within ~80 μm lateral to the central canal), the intermediate zone where the intercalated nucleus is located (between the medial and lateral zones), and the lateral zone where the IML column is located (within ~80 μm medial to the gray/white matter interface) (Heise, 2009). The number of GFP$^+$ neuronal cell bodies in each region of interest was counted with ImageJ. Briefly, Z stacks were compressed to create one MIP. Positive staining in a region of interest was selected using the threshold tool in ImageJ, and then the image was binarized. PRV$^+$ neurons were counted in each region using the “analyze particles” function, with size limit of 10 μm-400 μm (Figure 1E).

CGRP$^+$ axon analysis—To visualize nociceptive primary afferent fibers below the major sympathetic output, spinal level L4 was immunostained for CGRP and DRAQ5 nuclear dye. Ten-step Z stacks of 1 μm increments spanning 10 μm were acquired using a Leica TCS SP8 confocal microscope with 20 X magnification and 1.28 X optical zoom (25.6 X final magnification). Tiling with automatic stitching was used to generate a high-resolution image covering the whole section. Imaging parameters were kept consistent to minimize intensity variability. Z stacks were compressed to create one MIP and converted to a grayscale image (Figures 2 and 6). Using the Allen Mouse Spinal Cord Atlas and the DRAQ5$^+$ channel, spinal lamina I-II, III-V, and X were outlined on each image using the freehand selection tool in ImageJ. The image was converted to 8-bit format. The area of CGRP$^+$ staining in each region of interest was selected using the threshold tool in ImageJ and expressed as a percentage of the lamina area. The area of CGRP$^+$ axons in lamina I-II and III-V was the average of the left and right dorsal horn. The line tool in ImageJ was used to trace the longest axon in the left and right dorsal horn, and the lengths averaged to obtain one data point per section. The filaments tracer tool in Imaris v.8.1 (Bitplane) was used to generate a three-dimensional visualization of CGRP$^+$ axons in the dorsal horn (Figures 2A’–C’).

FosB$^+$ neuron analysis—FosB immunostaining is often used to define endogenous neuronal activity (Lyons and West, 2011). Therefore, to obtain a readout for neuronal activity, sections cut at spinal level T7 were immunostained for FosB, imaged, and then quantified. Ten-step Z stacks of 2 μm increments spanning the 20 μm were acquired using a Leica TCS SP8 confocal microscope with 20 X Magnification. Tiling with automatic stitching was used to generate a high-resolution image covering the whole section. Z stacks were compressed to create one MIP and converted to a gray scale image. Using the Allen Mouse Spinal Cord Atlas, spinal lamina I-IV and V-X were outlined on each image using

the freehand selection tool in ImageJ. Positive staining in each region of interest was selected using the threshold tool. The image was then binarized and the number of $FosB^+$ neurons per region was quantified using the "analyze particles" function, with size limit of 10–400 μm (Figure 3).

Spontaneous AD

Surgical implantation of telemetry probes: Telemetry transmitters were implanted into mice as described previously (Zhang et al., 2013). Briefly, 7 d before SCI, mice were anesthetized by injecting a mixture of ketamine (80 mg/kg) and xylazine (40 mg/kg) into the peritoneum. PA-C10 transmitters (Data Sciences International) were implanted via cannulation of the left common carotid artery, and the battery positioned in a skin pocket under the left flank. The neck skin was sutured closed. Mice were supplemented with 1 cc of saline and allowed to recover from anesthesia in warmed cages (~34°C) overnight.

Detection of AD events: Dataquest data acquisition software (Data Sciences International) was used to continuously record blood pressure (BP) and heart rate (HR). BP and HR were recorded for 2 days before SCI (baseline) and from 5 dpi to 30 dpi, with each data point representing the mean of one 5 s interval. MATLAB was used to create an algorithm to detect spontaneous AD events. The algorithm was based on the semi-automated method developed by Zhang et al. (2013), but incorporates validation steps to improve objectivity and efficiency. To validate the automated algorithm, the same data were analyzed using both the semi-automated and fully automated techniques and yielded similar results. The fully automated MATLAB AD detection algorithm is available upon request. For telemetry experiments in this study, a positive AD event was registered if BP increased > 20 mmHg above baseline, HR decreased > 30 bpm below baseline, and these events overlapped for > 66% of the time. *In vivo* telemetry experiments to determine the effect of GBP were repeated twice, each time with n = 7–8 mice per group. The experiment using α2δ−1 transgenic mice was an independent study and due to husbandry issues and high mortality in this strain, a replication was not attempted (Figures 4A–4D).

Induced AD

Colorectal distension (CRD): To measure cardiovascular responses elicited by visceral stimulation, CRD was performed at 35 dpi on one cohort of SCI implanted with telemetry probes and given saline or GBP. CRD was accomplished using a 4-French, 60 mm balloon-tipped catheter (Swan-Ganz monitoring catheter model 116F4; Edward Life Sciences). The catheter line was inserted into the rectum and the balloon positioned 1.5 cm from the anal opening. The catheter was secured to the tail with surgical tape. After securing the catheter, mice were left to acclimate for at least 20 min. After ensuring that the HR and BP traces were stable for 10 mins, the balloon was inflated with 0.3 mL air. Distention was maintained for 1 min before the balloon was deflated; the probe remained in the rectum. The procedure was repeated two more times, with a 10 min rest between stimulations. Pre-stimulation data were defined as the average HR and BP recorded in the 1 min immediately preceding stimulation. The post-stimulation data were defined as the maximum HR and minimum BP recorded during and in the 3 mins following CRD. The pre-stimulation and post-stimulation values for each mouse were averaged over three trials (Figures 4E–4G).

Cutaneous pinch (CP): To measure cardiovascular responses elicited by somatosensory stimulation, CP was performed at 35 dpi on one cohort of SCI mice implanted with telemetry probes and given saline or GBP. The tips of Hartman hemostats shielded with polyethylene tubing were used to pinch the flank just rostral to the hip joint. After ensuring that HR and BP traces were stable for 10 mins, the hemostat was closed to the first click for 30 s. The procedure was repeated once more, with a 5 min rest period between stimulations. Pre-stimulation data were defined as the average HR and BP recorded in the 1 min immediately preceding stimulation. The post-stimulation data were defined as the maximum HR and minimum BP recorded during, and in the 3 mins following CRD. The pre-stimulation and post-stimulation values for each mouse were averaged over two trials (Figures 4H–4J).

Splenic atrophy and lymphopenia—After administering the perfusion dose of anesthetic (see above), but before transcardial perfusion, fresh spleens were dissected and weighed. To control for differences in weight between sham and SCI mice, the spleen weight was expressed as a percentage of mouse body weight. Spleens then were post-fixed in 4% PFA overnight at 4°C, washed in 0.2 M phosphate buffer, then cryopreserved for 48 hours in 30% sucrose in 0.1 M PBS. Spleens were cut into 20 μm sections along the perpendicular axis in 1:10 series using a Microm HM 505E Digital Cryostat. Sections were collected onto SuperFrost slides and stored at −20°C until immunostaining. Sections were immunostained for CD3, B220 and DRAQ5. Five-step Z stacks of 2 μm increments spanning 10 μm were acquired using a Leica TCS SP8 confocal microscope with 20 X magnification and 1.28 X optical zoom (25.6x final magnification). Tiling with automatic stitching was used to generate a high-resolution image covering the whole section. Imaging parameters were consistent to minimize intensity variability. Z stack steps were compressed to create one MIP and the image converted to gray scale. Staining areas for CD3 or B220 were selected using the threshold tool and binarized in ImageJ. The area of CD3 or B220 positive staining was quantified using the *Measure Area* function in ImageJ then expressed as a percentage of the total spleen area (Figure 5; Figure S8).

QUANTIFICATION AND STATISTICAL ANALYSIS

Data involving comparison between two groups were analyzed with Student’s two-sided t tests. Data involving multiple independent groups were analyzed with parametric one-way ANOVA with Dunnett, Bonferroni, or the Kruskall-Wallis non-parametric one-way ANOVA with Dunn’s post hoc tests, as specified in individual figure legends. Two-Way ANOVA was used to analyze data with more than two groups of independent variables, with Dunnett or Bonferroni post hoc tests as specified in the figure legends. Heart rate and blood pressure data from the two radiotelemetry experiments testing the effect of GBP on spontaneous AD were pooled then analyzed using a mixed effect model, incorporating repeated-measures for each mouse, followed by slope comparison. We included ‘group’ as a fixed factor, ‘mouse’ as a random factor, and ‘experiment’ as an adjusting factor in this model. To compare the average number of daily events between SCI + saline and SCI + GBP groups, the average daily frequency of AD events for all mice was calculated (7.83 events per day), rounded to 8 AD events, and the percent of mice in each group that had > 8 or < 8 AD events per day was compared using a Chi-square test. The same method was used to compare the average daily

frequency of AD events in α2δ−1 WT and α2δ−1 TG mice, which yielded a cutoff of < 9 or > 9 AD events per day. Linear regression analysis was used to correlate: 1) the number of PRV^+ neurons with AD events (Figures S6A–S6C), 2) sprouting of $CGRP^+$ fibers with AD events (Figures S6D–S6F), 3) excitatory synapses with lymphocyte numbers (Figure S8I), and 4) $CGRP^+$ fibers with lymphocyte numbers (Figures S8J–S8M). All data are expressed as mean (with SEM) and statistical significance determined at $p < 0.05$. Group sizes were determined *a priori* to produce a power of 0.8 to reduce Type II errors.

Principal component analysis (PCA)—Multivariate data were reduced to principal components in RStudio with principal component analysis (PCA) prcomp arguments, and packages corrplot, devtools, factoextra, factoMineR, ggplot2, and dplyr (Figure 7). Prcomp runs a singular value decomposition of the data matrix. For the first PCA experiment (Figures 7A, 7C, 7E), outcome measures included PRV^+ neurons projecting to the spleen, CGRP area in lamina I-II, lamina III-V, lamina X, longest $CGRP^+$ axon, spleen weight, and autonomic dysreflexia recordings (taking the maximum number of AD events in the last 10 d of recording). These data were collated from saline or GBP-treated mice (with 35 d end points). To avoid listwise deletion and ensure a conservative analysis of the data, grand means were used to impute data for mice that did not have PRV^+ neuron counts (11/14 saline, 13/16 GBP mice), CGRP (11/14 saline, 13/16 GBP mice), or spleen weight data (5/14 saline, 9/16 GBP mice) (Nielson et al., 2020). For the second PCA experiment (Figures 7B, 7D, 7F), outcome measures were collated from an independent set of SCI + saline or SCI + GBP mice, with experimental end points of 28 dpi (no treatment withdrawal), 35 dpi (no treatment withdrawal), 42 dpi (14 d treatment withdrawal) or 56 dpi (28 d treatment withdrawal). These outcome measures included spleen $B220^+$ area, spleen $CD3^+$ area, excitatory synapses in T6-T9, CGRP area in lamina I-II, lamina III-V, lamina X, longest $CGRP^+$ axon, and α2δ−1 protein expression in T7. To avoid listwise deletion, grand means were used to impute data for mice that did not have α2δ−1 protein expression data (8/33 saline, 8/30 GBP mice) (Nielson et al., 2020). PC scores for each animal were exported to Microsoft Excel. Prediction ellipses are 99% confidence intervals.

Supplementary Material

Refer to Web version on PubMed Central for supplementary material.

ACKNOWLEDGMENTS

This work is supported by DOD W81XWH-13-1-0358 (to P.G.P.), the Craig H. Neilsen Foundation (457267 to F.H.B.), Wings for Life (to F.H.B. and P.G.P.), the National Institutes of Health (R01NS099532, R01NS083942, and R35NS111582 to P.G.P.), and the Ray W. Poppleton Endowment (to P.G.P.). The pseudorabies virus was supplied by the NIH Center for Neuroanatomy with Neurotropic Viruses (CNNV) with support from an NIH Virus Center grant (P40OD010996). The authors acknowledge Wenmin Lai, Ping Wei, Lori Hudson, and Katherine E. Wehde for technical assistance. The graphical abstract was created with BioRender.

REFERENCES

Ackery AD, Norenberg MD, and Krassioukov A (2007). Calcitonin gene-related peptide immunoreactivity in chronic human spinal cord injury. Spinal Cord 45, 678–686. [PubMed: 17339890]

Anderson KD (2004). Targeting recovery: priorities of the spinal cord-injured population. J. Neurotrauma 21, 1371–1383. [PubMed: 15672628]

Bauer CS, Nieto-Rostro M, Rahman W, Tran-Van-Minh A, Ferron L, Douglas L, Kadurin I, Sri Ranjan Y, Fernandez-Alacid L, Millar NS, et al. (2009). The increased trafficking of the calcium channel subunit alpha-2-delta-1 to presynaptic terminals in neuropathic pain is inhibited by the alpha-2-delta ligand pregabalin. J. Neurosci. 29, 4076–4088. [PubMed: 19339603]

Bikbaev A, Ciuraszkiewicz-Wojciech A, Heck J, Klatt O, Freund R, Mitlöhner J, Enrile Lacalle S, Sun M, Repetto D, Frischknecht R, et al. (2020). Auxiliary α2δ1 and α2δ3 Subunits of Calcium Channels Drive Excitatory and Inhibitory Neuronal Network Development. J. Neurosci. 40, 4824–4841. [PubMed: 32414783]

Boroujerdi A, Zeng J, Sharp K, Kim D, Steward O, and Luo ZD (2011). Calcium channel alpha-2-delta-1 protein upregulation in dorsal spinal cord mediates spinal cord injury-induced neuropathic pain states. Pain 152, 649–655. [PubMed: 21239111]

Brommer B, Engel O, Kopp MA, Watzlawick R, Müller S, Prüss H, Chen Y, DeVivo MJ, Finkenstaedt FW, Dirnagl U, et al. (2016). Spinal cord injury-induced immune deficiency syndrome enhances infection susceptibility dependent on lesion level. Brain 139, 692–707. [PubMed: 26754788]

Brown A, and Jacob JE (2006). Genetic approaches to autonomic dysreflexia. Prog. Brain Res. 152, 299–313. [PubMed: 16198709]

Cameron AA, Smith GM, Randall DC, Brown DR, and Rabchevsky AG (2006). Genetic manipulation of intraspinal plasticity after spinal cord injury alters the severity of autonomic dysreflexia. J. Neurosci. 26, 2923–2932. [PubMed: 16540569]

Cano G, Sved AF, Rinaman L, Rabin BS, and Card JP (2001). Characterization of the central nervous system innervation of the rat spleen using viral transneuronal tracing. J. Comp. Neurol. 439, 1–18. [PubMed: 11579378]

Chen J, Li L, Chen SR, Chen H, Xie JD, Sirrieh RE, MacLean DM, Zhang Y, Zhou MH, Jayaraman V, and Pan HL (2018). The α2δ−1-NMDA Receptor Complex Is Critically Involved in Neuropathic Pain Development and Gabapentin Therapeutic Actions. Cell Rep. 22, 2307–2321. [PubMed: 29490268]

Christopherson KS, Ullian EM, Stokes CC, Mullowney CE, Hell JW, Agah A, Lawler J, Mosher DF, Bornstein P, and Barres BA (2005). Thrombospondins are astrocyte-secreted proteins that promote CNS synaptogenesis. Cell 120, 421–433. [PubMed: 15707899]

Cole RL, Lechner SM, Williams ME, Prodanovich P, Bleicher L, Varney MA, and Gu G (2005). Differential distribution of voltage-gated calcium channel alpha-2 delta (alpha2delta) subunit mRNA-containing cells in the rat central nervous system and the dorsal root ganglia. J. Comp. Neurol. 491, 246–269. [PubMed: 16134135]

Ditunno JF, Little JW, Tessler A, and Burns AS (2004). Spinal shock revisited: a four-phase model. Spinal Cord 42, 383–395. [PubMed: 15037862]

Dolphin AC (2013). The α2δ subunits of voltage-gated calcium channels. Biochim. Biophys. Acta 1828, 1541–1549. [PubMed: 23196350]

Dutta S, and Sengupta P (2016). Men and mice: Relating their ages. Life Sci. 152, 244–248. [PubMed: 26596563]

Eldahan KC, Williams HC, Cox DH, Gollihue JL, Patel SP, and Rabchevsky AG (2020). Paradoxical effects of continuous high dose gabapentin treatment on autonomic dysreflexia after complete spinal cord injury. Exp. Neurol. 323, 113083. [PubMed: 31678138]

Eroglu C, Allen NJ, Susman MW, O'Rourke NA, Park CY, Ozkan E, Chakraborty C, Mulinyawe SB, Annis DS, Huberman AD, et al. (2009). Gabapentin receptor alpha2delta-1 is a neuronal thrombospondin receptor responsible for excitatory CNS synaptogenesis. Cell 139, 380–392. [PubMed: 19818485]

Failli V, Kopp MA, Gericke C, Martus P, Klingbeil S, Brommer B, Laginha I, Chen Y, DeVivo MJ, Dirnagl U, and Schwab JM (2012). Functional neurological recovery after spinal cord injury is impaired in patients with infections. Brain 135, 3238–3250. [PubMed: 23100450]

Faulkner JR, Herrmann JE, Woo MJ, Tansey KE, Doan NB, and Sofroniew MV (2004). Reactive astrocytes protect tissue and preserve function after spinal cord injury. J. Neurosci. 24, 2143–2155. [PubMed: 14999065]

Fenollosa P, Pallares J, Cervera J, Pelegrin F, Inigo V, Giner M, and Forner V (1993). Chronic pain in the spinal cord injured: statistical approach and pharmacological treatment. Paraplegia 31, 722–729. [PubMed: 7507585]

Ferguson AR, Stück ED, and Nielson JL (2011). Syndromics: a bioinformatics approach for neurotrauma research. Transl. Stroke Res. 2, 438–454. [PubMed: 22207883]

Field MJ, Cox PJ, Stott E, Melrose H, Offord J, Su TZ, Bramwell S, Corradini L, England S, Winks J, et al. (2006). Identification of the alpha-2-delta-1 subunit of voltage-dependent calcium channels as a molecular target for pain mediating the analgesic actions of pregabalin. Proc. Natl. Acad. Sci. USA 103, 17537–17542. [PubMed: 17088553]

Fitzpatrick MA, Suda KJ, Safdar N, Burns SP, Jones MM, Poggensee L, Ramanathan S, and Evans CT (2018). Changes in bacterial epidemiology and antibiotic resistance among veterans with spinal cord injury/disorder over the past 9 years. J. Spinal Cord Med. 41, 199–207. [PubMed: 28198662]

Friciu M, Roullin VG, and Leclair G (2017). Stability of gabapentin in extemporaneously compounded oral suspensions. PLoS ONE 12, e0175208. [PubMed: 28414771]

Gee NS, Brown JP, Dissanayake VU, Offord J, Thurlow R, and Woodruff GN (1996). The novel anticonvulsant drug, gabapentin (Neurontin), binds to the alpha2delta subunit of a calcium channel. J. Biol. Chem. 271, 5768–5776. [PubMed: 8621444]

Gong HC, Hang J, Kohler W, Li L, and Su TZ (2001). Tissue-specific expression and gabapentin-binding properties of calcium channel alpha2delta subunit subtypes. J. Membr. Biol. 184, 35–43. [PubMed: 11687876]

Guttmann L, and Whitteridge D (1947). Effects of bladder distension on autonomic mechanisms after spinal cord injuries. Brain 70, 361–404. [PubMed: 18903252]

Hagen EM, and Rekand T (2015). Management of Neuropathic Pain Associated with Spinal Cord Injury. Pain Ther. 4, 51–65. [PubMed: 25744501]

Heise C (2009). Atlas of the mouse spinal cord. In The Spinal Cord, Watson C, Paxinos G, and Kayalioglu G, eds. (Academic Press), pp. 308–379.

Hendrich J, Van Minh AT, Heblich F, Nieto-Rostro M, Watschinger K, Striessnig J, Wratten J, Davies A, and Dolphin AC (2008). Pharmacological disruption of calcium channel trafficking by the alpha2delta ligand gabapentin. Proc. Natl. Acad. Sci. USA 105, 3628–3633. [PubMed: 18299583]

Hotamisligil GS (2017). Inflammation, metaflammation and immunometabolic disorders. Nature 542, 177–185. [PubMed: 28179656]

Hou S, Duale H, Cameron AA, Abshire SM, Lyttle TS, and Rabchevsky AG (2008). Plasticity of lumbosacral propriospinal neurons is associated with the development of autonomic dysreflexia after thoracic spinal cord transection. J. Comp. Neurol. 509, 382–399. [PubMed: 18512692]

Ippolito DM, and Eroglu C (2010). Quantifying synapses: an immunocytochemistry-based assay to quantify synapse number. J. Vis. Exp. (45), 2270. [PubMed: 21113117]

Jackson SJ, Andrews N, Ball D, Bellantuono I, Gray J, Hachoumi L, Holmes A, Latcham J, Petrie A, Potter P, et al. (2017). Does age matter? The impact of rodent age on study outcomes. Lab. Anim. 51, 160–169. [PubMed: 27307423]

Jacob JE, Gris P, Fehlings MG, Weaver LC, and Brown A (2003). Autonomic dysreflexia after spinal cord transection or compression in 129Sv, C57BL, and Wallerian degeneration slow mutant mice. Exp. Neurol. 183, 136–146. [PubMed: 12957497]

Jansen AS, Nguyen XV, Karpitskiy V, Mettenleiter TC, and Loewy AD (1995). Central command neurons of the sympathetic nervous system: basis of the fight-or-flight response. Science 270, 644–646. [PubMed: 7570024]

Kellner Y, Gödecke N, Dierkes T, Thieme N, Zagrebelsky M, and Korte M (2014). The BDNF effects on dendritic spines of mature hippocampal neurons depend on neuronal activity. Front. Synaptic Neurosci. 6, 5. [PubMed: 24688467]

Kigerl KA, McGaughy VM, and Popovich PG (2006). Comparative analysis of lesion development and intraspinal inflammation in four strains of mice following spinal contusion injury. J. Comp. Neurol. 494, 578–594. [PubMed: 16374800]

Kigerl KA, Hall JC, Wang L, Mo X, Yu Z, and Popovich PG (2016). Gut dysbiosis impairs recovery after spinal cord injury. J. Exp. Med. 213, 2603–2620. [PubMed: 27810921]

Kitzman PH, Uhl TL, and Dwyer MK (2007). Gabapentin suppresses spasticity in the spinal cord-injured rat. Neuroscience 149, 813–821. [PubMed: 17964732]

Kopp MA, Watzlawick R, Martus P, Failli V, Finkenstaedt FW, Chen Y, DeVivo MJ, Dirnagl U, and Schwab JM (2017). Long-term functional outcome in patients with acquired infections after acute spinal cord injury. Neurology 88, 892–900. [PubMed: 28130472]

Krassioukov AV, and Weaver LC (1995). Reflex and morphological changes in spinal preganglionic neurons after cord injury in rats. Clin. Exp. Hypertens. 17, 361–373. [PubMed: 7735281]

Krenz NR, and Weaver LC (1998). Sprouting of primary afferent fibers after spinal cord transection in the rat. Neuroscience 85, 443–458. [PubMed: 9622243]

Krenz NR, Meakin SO, Krassioukov AV, and Weaver LC (1999). Neutralizing intraspinal nerve growth factor blocks autonomic dysreflexia caused by spinal cord injury. J. Neurosci. 19, 7405–7414. [PubMed: 10460247]

Kursh ED, Freehafer A, and Persky L (1977). Complications of autonomic dysreflexia. J. Urol. 118, 70–72. [PubMed: 17757]

Lee BS, Jun IG, Kim SH, and Park JY (2013). Intrathecal gabapentin increases interleukin-10 expression and inhibits pro-inflammatory cytokine in a rat model of neuropathic pain. J. Korean Med. Sci. 28, 308–314. [PubMed: 23399960]

Levendoglu F, Ogün CO, Ozerbil O, Ogün TC, and Ugurlu H (2004). Gabapentin is a first line drug for the treatment of neuropathic pain in spinal cord injury. Spine 29, 743–751. [PubMed: 15087796]

Li CY, Zhang XL, Matthews EA, Li KW, Kurwa A, Boroujerdi A, Gross J, Gold MS, Dickenson AH, Feng G, and Luo ZD (2006). Calcium channel alpha2delta1 subunit mediates spinal hyperexcitability in pain modulation. Pain 125, 20–34. [PubMed: 16764990]

Lindan R, Joiner E, Freehafer AA, and Hazel C (1980). Incidence and clinical features of autonomic dysreflexia in patients with spinal cord injury. Paraplegia 18, 285–292. [PubMed: 7443280]

Llewellyn-Smith IJ, and Weaver LC (2001). Changes in synaptic inputs to sympathetic preganglionic neurons after spinal cord injury. J. Comp. Neurol. 435, 226–240. [PubMed: 11391643]

Llewellyn-Smith IJ, Weaver LC, and Keast JR (2006). Effects of spinal cord injury on synaptic inputs to sympathetic preganglionic neurons. Prog. Brain Res. 152, 11–26. [PubMed: 16198690]

Lucin KM, Sanders VM, Jones TB, Malarkey WB, and Popovich PG (2007). Impaired antibody synthesis after spinal cord injury is level dependent and is due to sympathetic nervous system dysregulation. Exp. Neurol. 207, 75–84. [PubMed: 17597612]

Lucin KM, Sanders VM, and Popovich PG (2009). Stress hormones collaborate to induce lymphocyte apoptosis after high level spinal cord injury. J. Neurochem. 110, 1409–1421. [PubMed: 19545280]

Lyons MR, and West AE (2011). Mechanisms of specificity in neuronal activity-regulated gene transcription. Prog. Neurobiol. 94, 259–295. [PubMed: 21620929]

Malik AN, Vierbuchen T, Hemberg M, Rubin AA, Ling E, Couch CH, Stroud H, Spiegel I, Farh KK, Harmin DA, and Greenberg ME (2014). Genome-wide identification and characterization of functional neuronal activity-dependent enhancers. Nat. Neurosci. 17, 1330–1339. [PubMed: 25195102]

Matsushita M (1998). Ascending propriospinal afferents to area X (substantia grisea centralis) of the spinal cord in the rat. Exp. Brain Res. 119, 356–366. [PubMed: 9551836]

Mayorov DN, Adams MA, and Krassioukov AV (2001). Telemetric blood pressure monitoring in conscious rats before and after compression injury of spinal cord. J. Neurotrauma 18, 727–736. [PubMed: 11497098]

McNeill DL, Carlton SM, Coggeshall RE, and Hulsebosch CE (1990). Denervation-induced intraspinal synaptogenesis of calcitonin gene-related peptide containing primary afferent terminals. J. Comp. Neurol. 296, 263–268. [PubMed: 2358535]

Mironets E, Osei-Owusu P, Bracchi-Ricard V, Fischer R, Owens EA, Ricard J, Wu D, Saltos T, Collyer E, Hou S, et al. (2018). Soluble TNFα Signaling within the Spinal Cord Contributes to the Development of Autonomic Dysreflexia and Ensuing Vascular and Immune Dysfunction after Spinal Cord Injury. J. Neurosci. 38, 4146–4162. [PubMed: 29610439]

Nair AB, and Jacob S (2016). A simple practice guide for dose conversion between animals and human. J. Basic Clin. Pharm. 7, 27–31. [PubMed: 27057123]

Nielson JL, Cooper SR, Seabury SA, Luciani D, Fabio A, Temkin NR, and Ferguson AR; Track-TBI Investigators (2020). Statistical Guidelines for Handling Missing Data in Traumatic Brain Injury Clinical Research. J. Neurotrauma, Published online March 10, 2020. 10.1089/neu.2019.6702.

Prüss H, Tedeschi A, Thiriot A, Lynch L, Loughhead SM, Stutte S, Mazo IB, Kopp MA, Brommer B, Blex C, et al. (2017). Spinal cord injury-induced immunodeficiency is mediated by a sympathetic-neuroendocrine adrenal reflex. Nat. Neurosci. 20, 1549–1559. [PubMed: 28920935]

Putzke JD, Richards JS, Kezar L, Hicken BL, and Ness TJ (2002). Long-term use of gabapentin for treatment of pain after traumatic spinal cord injury. Clin. J. Pain 18, 116–121. [PubMed: 11882775]

Rabchevsky AG, Patel SP, Duale H, Lyttle TS, O'Dell CR, and Kitzman PH (2011). Gabapentin for spasticity and autonomic dysreflexia after severe spinal cord injury. Spinal Cord 49, 99–105. [PubMed: 20514053]

Rabchevsky AG, Patel SP, Lyttle TS, Eldahan KC, O'Dell CR, Zhang Y, Popovich PG, Kitzman PH, and Donohue KD (2012). Effects of gabapentin on muscle spasticity and both induced as well as spontaneous autonomic dysreflexia after complete spinal cord injury. Front. Physiol. 3, 329. [PubMed: 22934077]

Radulovic LL, Türck D, von Hodenberg A, Vollmer KO, McNally WP, DeHart PD, Hanson BJ, Bockbrader HN, and Chang T (1995). Disposition of gabapentin (neurontin) in mice, rats, dogs, and monkeys. Drug Metab. Dispos. 23, 441–448. [PubMed: 7600909]

Risher WC, and Eroglu C (2012). Thrombospondins as key regulators of synaptogenesis in the central nervous system. Matrix Biol. 31, 170–177. [PubMed: 22285841]

Risher WC, Kim N, Koh S, Choi JE, Mitev P, Spence EF, Pilaz LJ, Wang D, Feng G, Silver DL, et al. (2018). Thrombospondin receptor α2δ−1 promotes synaptogenesis and spinogenesis via postsynaptic Rac1. J. Cell Biol. 217, 3747–3765. [PubMed: 30054448]

Schmued LC, and Fallon JH (1986). Fluoro-Gold: a new fluorescent retrograde axonal tracer with numerous unique properties. Brain Res. 377, 147–154. [PubMed: 2425899]

Sun W, Larson MJ, Kiyoshi CM, Annett AJ, Stalker WA, Peng J, and Tedeschi A (2020). Gabapentinoid treatment promotes corticospinal plasticity and regeneration following murine spinal cord injury. J. Clin. Invest. 130, 345–358. [PubMed: 31793909]

Tai Q, Kirshblum S, Chen B, Millis S, Johnston M, and DeLisa JA (2002). Gabapentin in the treatment of neuropathic pain after spinal cord injury: a prospective, randomized, double-blind, crossover trial. J. Spinal Cord Med. 25, 100–105. [PubMed: 12137213]

Tanabe M, Ono K, Honda M, and Ono H (2009). Gabapentin and pregabalin ameliorate mechanical hypersensitivity after spinal cord injury in mice. Eur. J. Pharmacol. 609, 65–68. [PubMed: 19285498]

Tedeschi A, Dupraz S, Laskowski CJ, Xue J, Ulas T, Beyer M, Schultze JL, and Bradke F (2016). The Calcium Channel Subunit Alpha2delta2 Suppresses Axon Regeneration in the Adult CNS. Neuron 92, 419–434. [PubMed: 27720483]

To TP, Lim TC, Hill ST, Frauman AG, Cooper N, Kirsa SW, and Brown DJ (2002). Gabapentin for neuropathic pain following spinal cord injury. Spinal Cord 40, 282–285. [PubMed: 12037709]

Ueno M, Ueno-Nakamura Y, Niehaus J, Popovich PG, and Yoshida Y (2016). Silencing spinal interneurons inhibits immune suppressive autonomic reflexes caused by spinal cord injury. Nat. Neurosci. 19, 784–787. [PubMed: 27089020]

Wang X, Chen W, Liu W, Wu J, Shao Y, and Zhang X (2009). The role of thrombospondin-1 and transforming growth factor-beta after spinal cord injury in the rat. J. Clin. Neurosci. 16, 818–821. [PubMed: 19342245]

Warner FM, Cragg JJ, Jutzeler CR, Röhrich F, Weidner N, Saur M, Maier DD, Schuld C, EMSCI Sites; Curt A, and Kramer JK (2017). Early Administration of Gabapentinoids Improves Motor Recovery after Human Spinal Cord Injury. Cell Rep. 18, 1614–1618. [PubMed: 28199834]

Weaver LC, Cassam AK, Krassioukov AV, and Llewellyn-Smith IJ (1997). Changes in immunoreactivity for growth associated protein-43 suggest reorganization of synapses on spinal sympathetic neurons after cord transection. Neuroscience 81, 535–551. [PubMed: 9300440]

Weaver LC, Verghese P, Bruce JC, Fehlings MG, Krenz NR, and Marsh DR (2001). Autonomic dysreflexia and primary afferent sprouting after clip-compression injury of the rat spinal cord. J. Neurotrauma 18, 1107–1119. [PubMed: 11686496]

Yang JY, Lee WI, Shin WK, Kim CH, Baik SW, and Kim KH (2013). Administration of four different doses of gabapentin reduces awakening from breakthrough pain and adverse effects in outpatients with neuropathic pain during the initial titration. Korean J. Anesthesiol. 65, 48–54. [PubMed: 23904939]

Zagon A, and Smith AD (1993). Monosynaptic projections from the rostral ventrolateral medulla oblongata to identified sympathetic preganglionic neurons. Neuroscience 54, 729–743. [PubMed: 8332259]

Zeng J, Kim D, Li KW, Sharp K, Steward O, Zaucke F, and Luo ZD (2013). Thrombospondin-4 contributes to spinal cord injury-induced changes in nociception. Eur. J. Pain 17, 1458–1464. [PubMed: 23649982]

Zhang Y, Guan Z, Reader B, Shawler T, Mandrekar-Colucci S, Huang K, Weil Z, Bratasz A, Wells J, Powell ND, et al. (2013). Autonomic dysreflexia causes chronic immune suppression after spinal cord injury. J. Neurosci. 33, 12970–12981. [PubMed: 23926252]

Zinck ND, Rafuse VF, and Downie JW (2007). Sprouting of CGRP primary afferents in lumbosacral spinal cord precedes emergence of bladder activity after spinal injury. Exp. Neurol. 204, 777–790. [PubMed: 17331502]

Zour E, Lodhi SA, Nesbitt RU, Silbering SB, and Chaturvedi PR (1992). Stability studies of gabapentin in aqueous solutions. Pharm. Res. 9, 595–600. [PubMed: 1608888]

Highlights

- Prophylactic GBP blocks synaptogenesis and autonomic fiber sprouting after SCI in mice
- Prophylactic GBP prevents autonomic dysreflexia and immune suppression
- Benefits of prophylactic GBP persist at least 1 month after treatment withdrawal
- Syndromic analyses predict spinal sympathetic reflex pathology and GBP efficacy

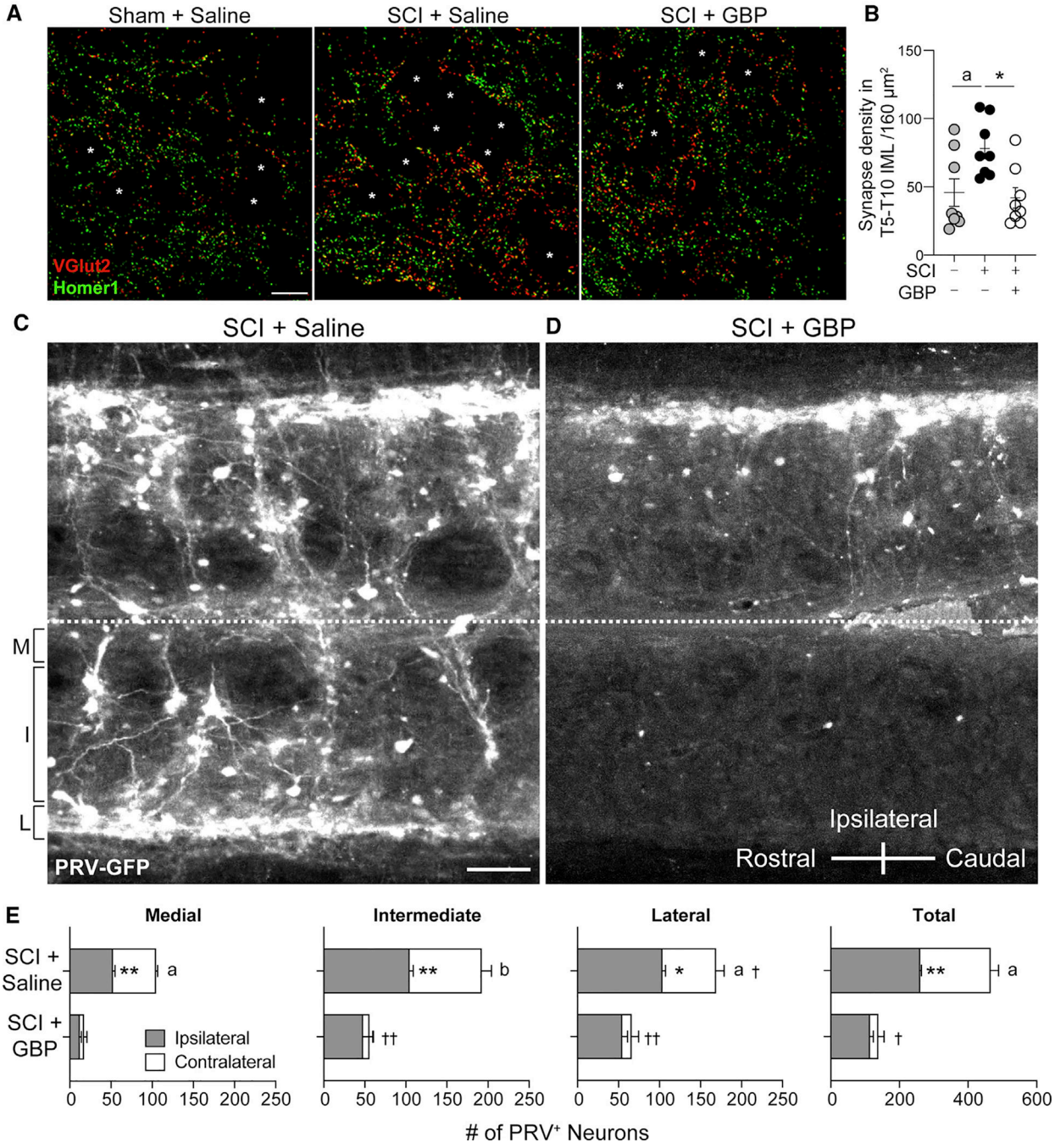

Figure 1. Prophylactic GBP (pGBP) prevents excitatory synaptogenesis and limits structural plasticity in autonomic circuitry at 35 dpi

(A) Representative images of VGlut2^{+}Homer1^{+} synapses in the IML (spinal level T9). The location of Fluoro-Gold^{+} SPN somata is marked by asterisks. Scale bar, 20 µm.

(B) Total number of synapses in the IML at T5–T10 spinal levels increases after SCI. This is blocked by pGBP. One-way ANOVA with Bonferroni post hoc test, n=8 mice/group, $^{a}p < 0.05$ versus sham + saline, *$p < 0.05$ for SCI + saline versus SCI + GBP, mean ± SEM. See also Figures S1 and S5.

(C–E) Spinal-splenic circuitry labeled retrogradely via intrasplenic injection of PRV-GFP. The compass (D) indicates spleen position. Dashed line, central canal. (C and D) Representative horizontal sections of T4–T5 spinal cord in SCI + saline (C) or SCI + GBP (D) mice. Scale bar (in C), 100 μm.

(E) pGBP significantly reduced the number of PRV^+ neurons in the medial (M), intermediate (I), and lateral (L) gray matter in SCI mice compared with saline-treated SCI mice. Two-way ANOVA with Bonferroni multiple comparisons; n = 3 mice/group; $^*p < 0.05$, $^{**}p < 0.01$ comparing ipsilateral sides between groups; $^ap < 0.01$, $^bp < 0.001$ comparing contralateral sides between groups; †p < 0.05, ††p < 0.01 comparing ipsilateral with contralateral sides within groups; mean + SEM. See also Figure S6.

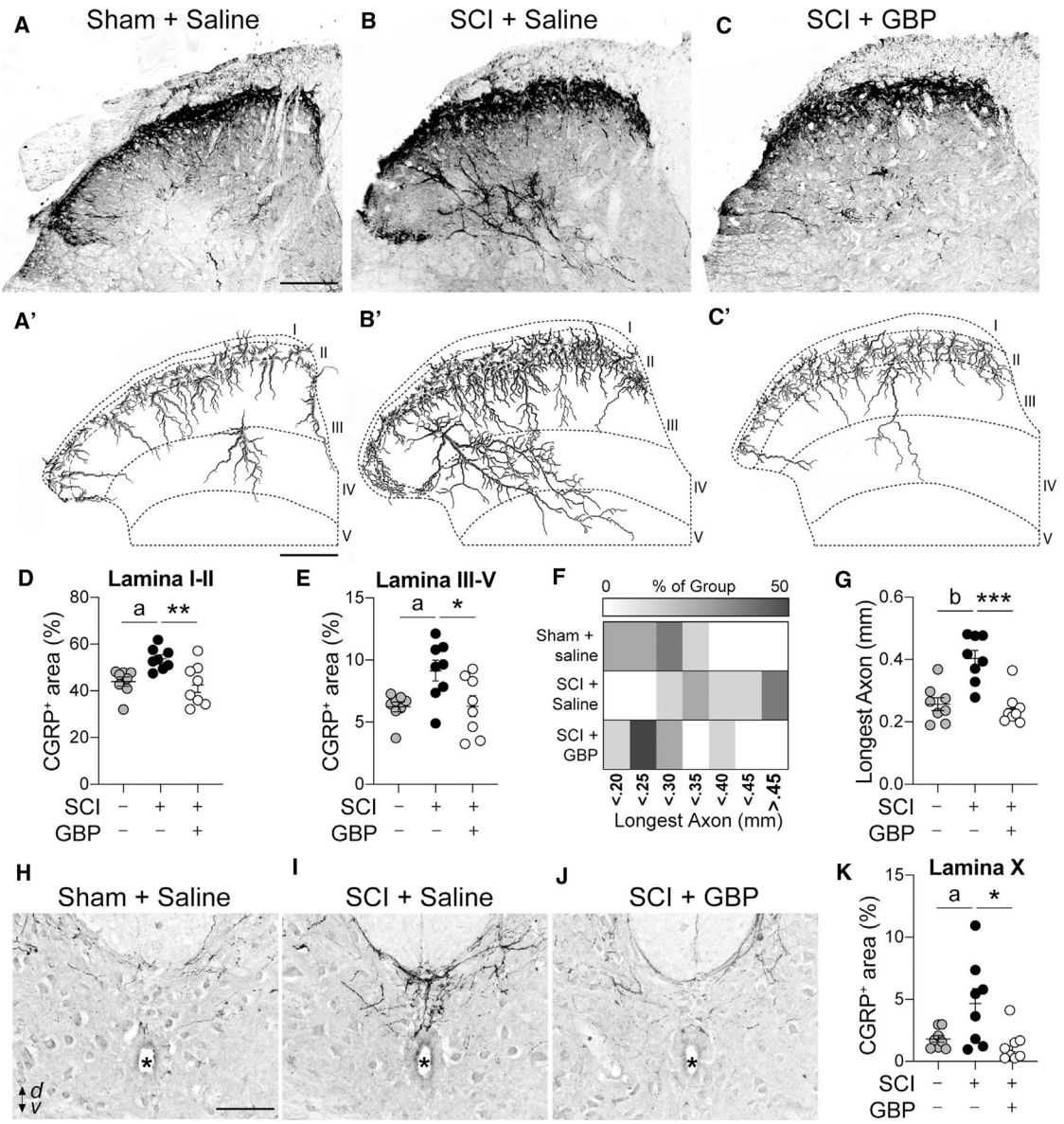

Figure 2. pGBP blocks CGRP$^+$ fiber sprouting in the lumbar spinal cord after SCI

(A–C) Representative grayscale confocal maximum intensity projections (MIPs) of CGRP immunostaining in the L4 dorsal horn from sham or SCI mice treated with saline or pGBP. Scale bar (in A), 130 μm.

(A'–C') Three-dimensional renderings of CGRP$^+$ axon profiles.

(D and E) SCI-induced sprouting of CGRP$^+$ fibers in laminae I–II (D) and laminae III–V (E) is blocked by pGBP.

(F) Heatmap showing the range of the longest CGRP$^+$ axon in the dorsal horn in sham or SCI mice given saline or pGBP.

(G) In SCI mice treated with pGBP, the length of the longest CGRP$^+$ axon was reduced significantly compared with SCI mice given saline.

(H–J) Representative MIPs of $CGRP^+$ axons in L4 lamina X from sham or SCI mice treated with saline or pGBP. Scale bar (in H), 100 μm. d: dorsal; v: ventral. Asterisks denote the central canal.

(K) pGBP blocks SCI-induced sprouting of lamina X $CGRP^+$ axons.

(D, E, G, and K) One-way ANOVA with Bonferroni post hoc tests; n = 8 mice/group; $^{a}p < 0.05$, $^{b}p < 0.001$ versus sham + saline; $^{*}p < 0.05$, $^{**}p < 0.01$, $^{***}p < 0.001$ for SCI + saline versus SCI + GBP; mean ± SEM.

See also Figures S5 and S6.

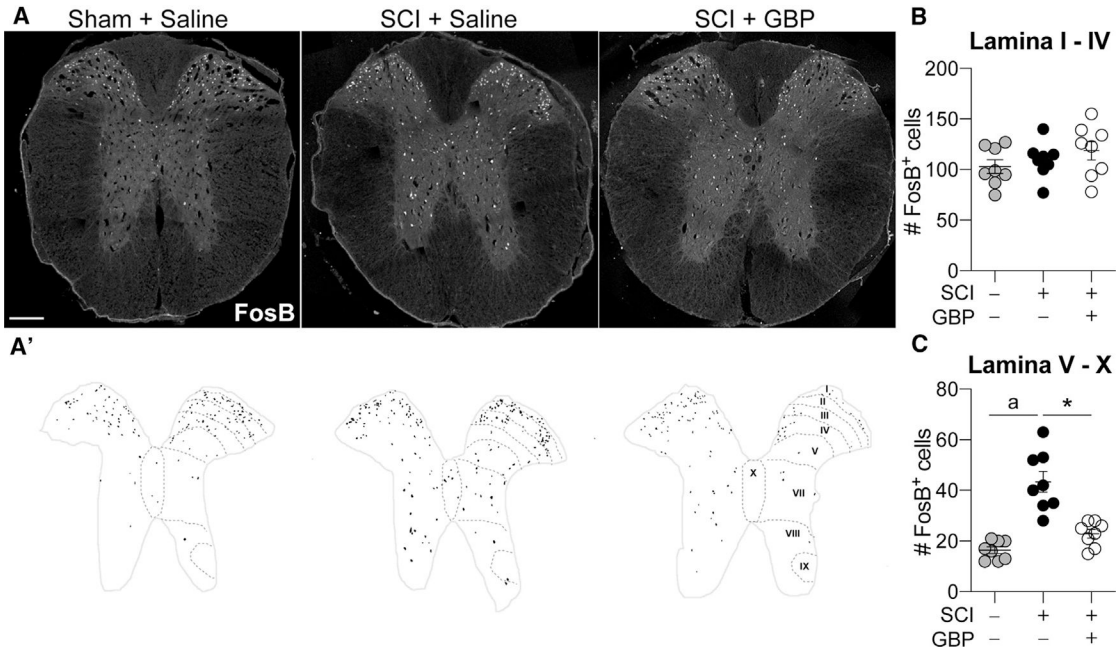

Figure 3. pGBP reduces the excitability of neurons in intermediate gray matter below the level of SCI

(A and A') Representative grayscale (top row) and inverted binarized (A') images of FosB-immunostained T8 spinal cord sections. Scale bar, 200 μm.

(B) Basal levels of $FosB^+$ neurons in laminae I–IV were unchanged after SCI with or without pGBP.

(C) In laminae V–X, SCI + saline mice had significantly more $FosB^+$ neurons relative to sham + saline mice; this effect was blocked by pGBP.

(B and C) Kruskal-Wallis one-way ANOVA with Dunn's multiple comparisons, n = 8 mice/group, $^a p < 0.0001$ versus sham + saline, $^* p < 0.05$ for SCI + saline versus SCI + GBP, mean ± SEM.

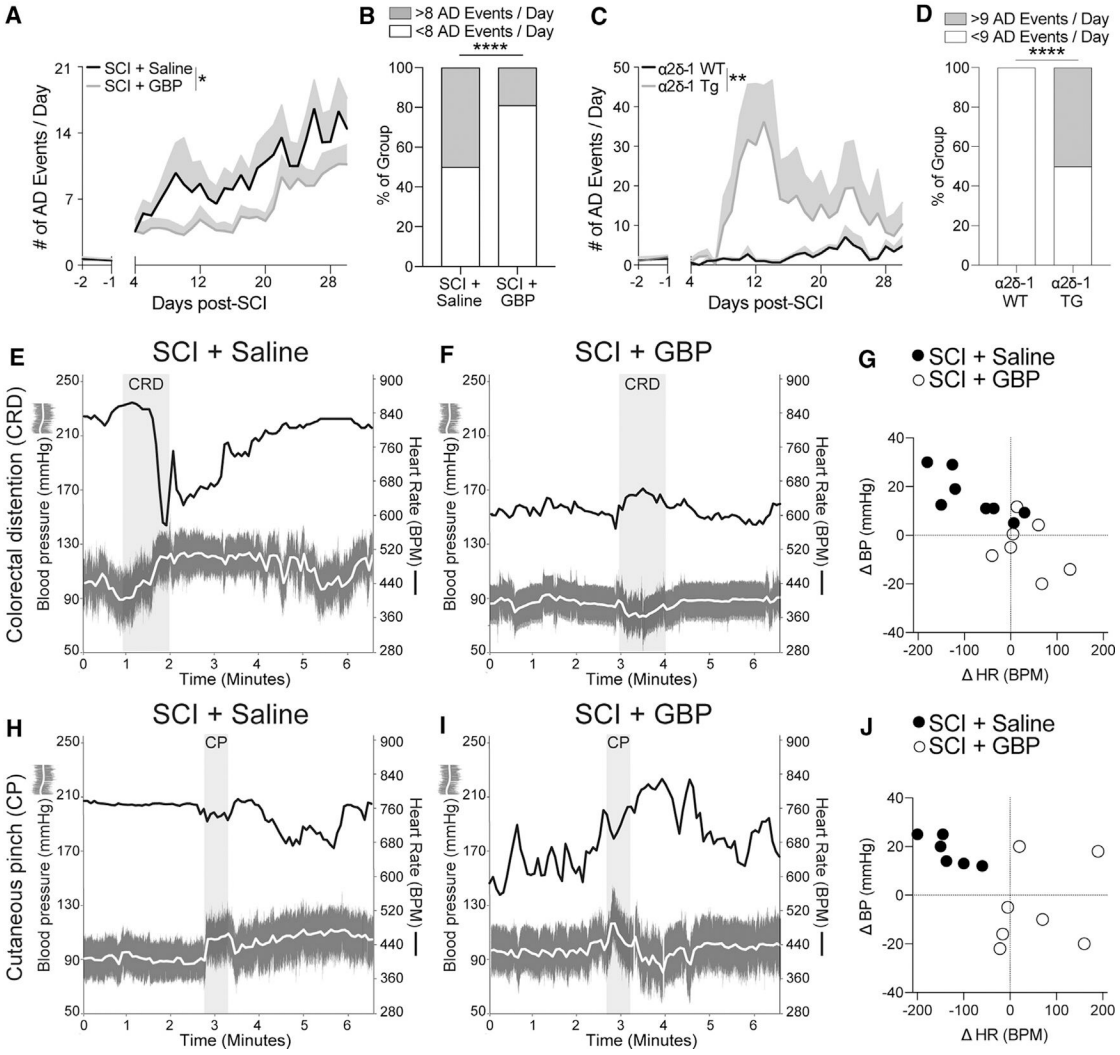

Figure 4. The frequency and severity of autonomic dysreflexia (AD) are reduced by pGBP

(A–B) Radiotelemetry monitoring of heart rate (HR) and blood pressure (BP) in SCI mice treated with saline or pGBP.

(A) In SCI mice treated with pGBP, AD onset was delayed, as was the frequency of daily AD events compared with SCI + saline control mice. Mixed effect models to compare slopes between groups; data were pooled from two experimental replicates, each with 7–8 mice/group for a total of SCI + saline (n = 14) and SCI + GBP (n = 16); *$p < 0.05$; mean + SEM. See also Figure S6.

(B) The percentage of mice that experienced more than 8 AD events/day was reduced significantly by pGBP.

(C and D) Telemetry recording of HR and BP in α2δ−1 TG and WT littermate control mice after SCI.

(C) The frequency of spontaneous daily AD after SCI was exacerbated in α2δ−1 TG mice compared with α2δ−1 WT controls. Two-way ANOVA with repeated-measures, n = 3–4 mice/group, **$p < 0.01$, mean + SEM.

(D) TG overexpression of α2δ−1 significantly increased the percentage of mice in each group that experienced more than 9 AD events/day.
(B and D) Chi-square test; SCI + saline, n = 14; SCI + GBP, n = 16; $^{****}p < 0.0001$.
(E–J) Pulsatile arterial BP (gray trace; mean, white line) and HR (mean, black line) recordings measured by *in vivo* radiotelemetry before, during, and after visceral stimulation (60-s colorectal distention, CRD; E–G) or somatosensory stimulation (30-s cutaneous pinch, CP; H–J). Representative HR/BP traces from SCI mice (35 dpi) in (G) and (J) are shown in (E), (F), (H), and (I).
(E and F) Before CRD stimulation, BP and HR were stable in all mice. During and in the 3 min after CRD, hypertension and bradycardia were elicited in SCI + saline mice. These cardiovascular changes could not be triggered in SCI + GBP mice.
(G) Mice treated with pGBP or saline are clustered distinctly based on CRD-induced changes in BP and HR.
(H and I) During and in the 3 min after CP, SCI + saline mice displayed hypertension and bradycardia. These changes were not observed in SCI + GBP mice.
(J) Mice treated with pGBP or saline are clustered distinctly based on CP-induced changes in BP and HR.

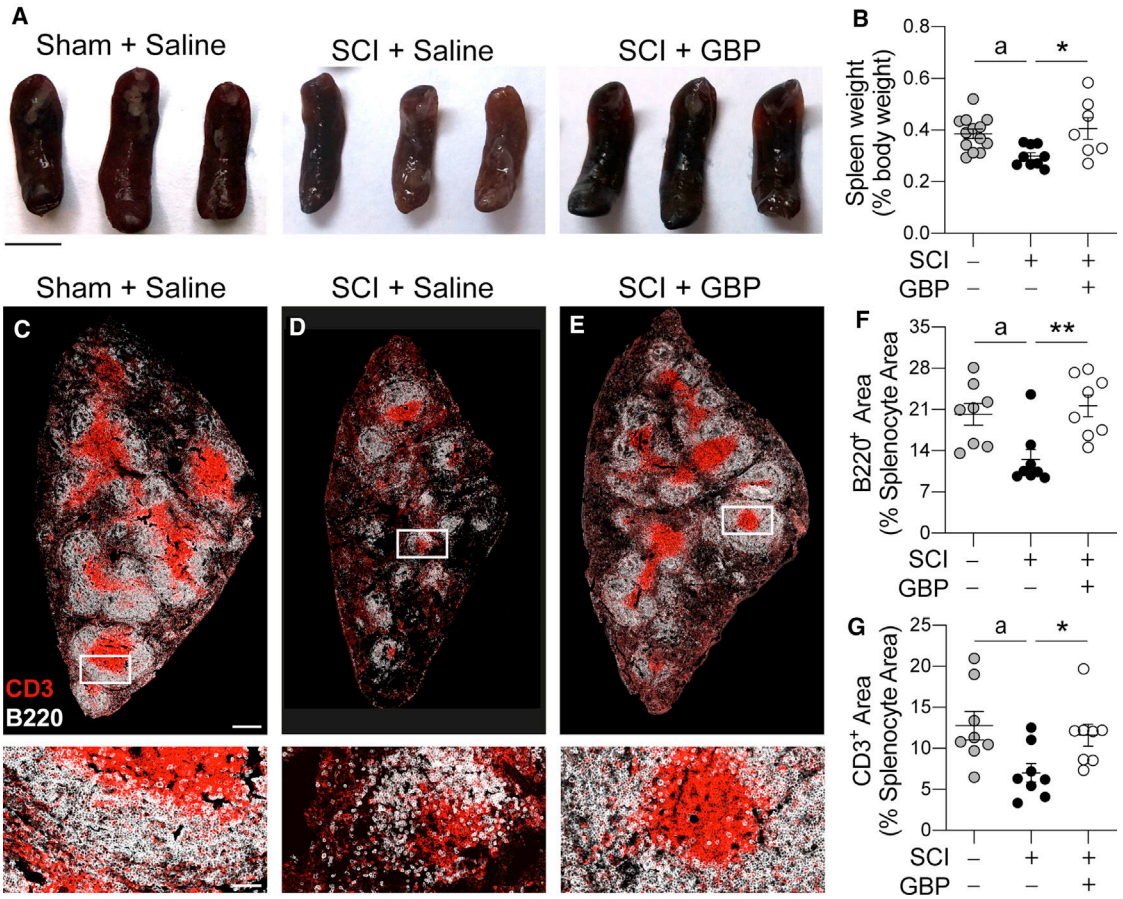

Figure 5. pGBP blocks splenic atrophy and leukopenia caused by T3 SCI

(A) Gross images of representative spleens from sham and SCI mice treated with saline or pGBP. Scale bar, 0.5 cm.

(B) SCI causes splenic atrophy, an effect that is blocked by pGBP. One-way ANOVA with Bonferroni post hoc test, n = 13 sham + saline, n = 9 SCI + saline, n = 7 SCI + GBP, $^{a}p < 0.05$ versus sham + saline, $^{*}p < 0.05$ for SCI + saline versus SCI + GBP, mean ± SEM.

(C–E) Representative cross-sections of spleens from sham and SCI mice treated with saline or pGBP stained for B220 (white) and CD3 (red). Higher-magnification insets reveal lymphocytes in a representative follicle. Scale bar (in C), 250 μm and 50 μm (insets in C–E).

(F and G) SCI reduces splenic $B220^{+}$ B lymphocytes (F) and $CD3^{+}$ T lymphocytes (G) compared with sham + saline controls. pGBP blocks SCI-induced depletion of splenic lymphocytes. One-way ANOVA with Bonferroni post hoc tests, n = 8 mice/group, $^{a}p < 0.05$ versus sham + saline, $^{*}p < 0.05$, $^{**}p < 0.01$ for SCI + saline versus SCI + GBP, mean ± SEM.

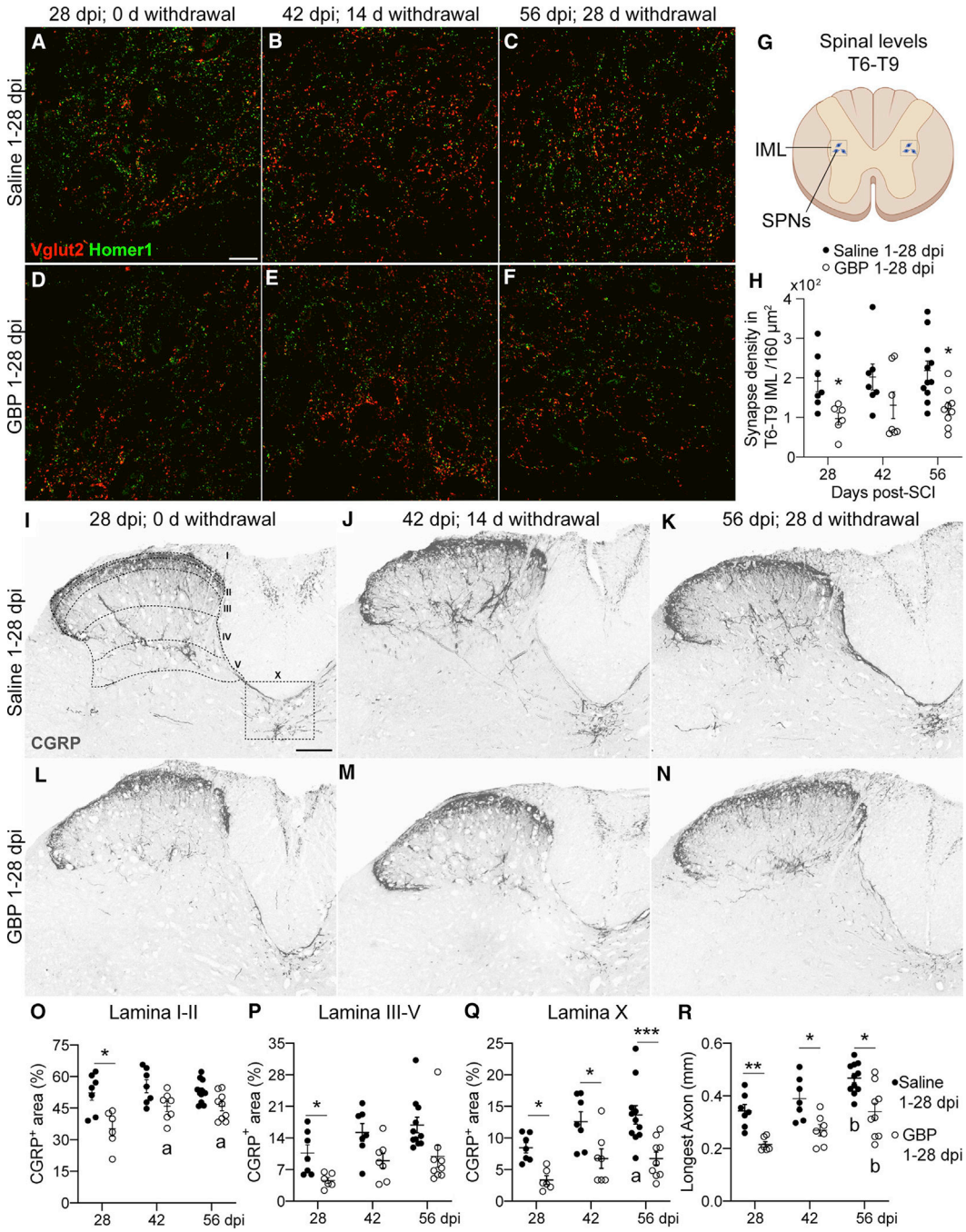

Figure 6. pGBP prevents excitatory synaptogenesis and CGRP afferent sprouting up to 28 days after treatment withdrawal

(A–F) Representative images of VGlut2 and Homer1 staining in T6–T9 IML of SCI mice treated with saline or pGBP and then perfused at 28 dpi (no withdrawal, A and D), 42 dpi (14 d withdrawal, B and E), or 56 dpi (28 d withdrawal, C and F). Scale bar (in A), 20 µm.

(G) Region of quantification.

(H) pGBP reduces excitatory synaptogenesis up to 56 dpi (28 days after GBP withdrawal).

(I–N) Representative images of $CGRP^+$ fibers in the dorsal horn of SCI mice treated with saline or pGBP and then perfused at 28 dpi (no withdrawal, I and L), 42 dpi (14 d withdrawal, J and M), or 56 dpi (28 d withdrawal, K and N). Scale bar (in I), 100 μm.
(O–R) pGBP significantly decreased the $CGRP^+$ area in all spinal laminae at 28 dpi (no withdrawal) but not after treatment withdrawal in superficial laminae I–II (O) or laminae III–V (P). However, pGBP did significantly reduce $CGRP^+$ axon sprouting into lamina X (Q) at 42 dpi (14 d withdrawal) and 56 dpi (28 d withdrawal).
(R) pGBP blocked $CGRP^+$ axon elongation into deep spinal laminae at 28 dpi (no withdrawal), 42 dpi (14 d withdrawal), and 56 dpi (28 d withdrawal).
(H and O–R) Two-way ANOVA with Bonferroni post hoc tests; n = 6–11 mice/group; $^*p < 0.05$, $^{**}p < 0.01$, $^{***}p < 0.001$ comparing treatment groups at matched time points; $^ap < 0.05$, $^bp < 0.01$ comparing within-group data to 28 dpi; mean ± SEM. There was no main effect of time post-injury for synapses ($p = 0.36$) but a main effect of time on $CGRP^+$ area in laminae I–II ($p = 0.049$), laminae III–V ($p = 0.031$), lamina X ($p = 0.019$), and $CGRP^+$ elongation ($p = 0.0007$). There was a main effect of pGBP on excitatory synapse number ($p = 0.0022$), $CGRP^+$ area in laminae I–II ($p < 0.0001$), laminae III–V ($p = 0.0008$), lamina X ($p < 0.0001$), and $CGRP^+$ elongation ($p < 0.0001$). There was no interaction between time and treatment group for any outcome measure.
See also Figure S8.

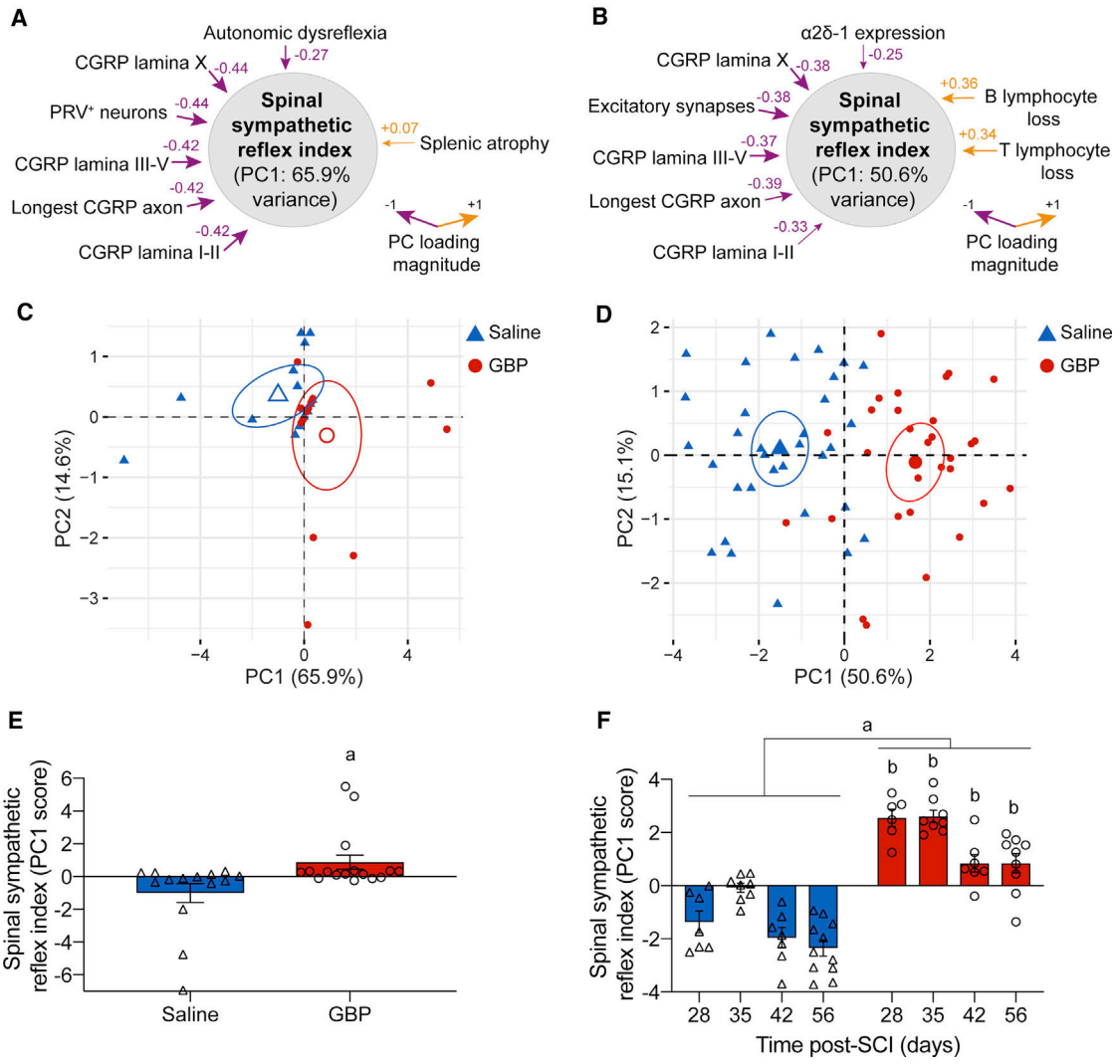

Figure 7. Principle-component analysis (PCA) predicts an impaired spinal sympathetic reflex index after SCI that is improved by pGBP

(A and B) Two PCA experiments organized multiple measures of structural plasticity and functional dysautonomia into a bivariate correlation matrix. This gives each outcome measure a loading range from negative (purple, −1) to positive (orange, +1). Principal component 1 (PC1), accounting for 65.9% and 50.6% of the variance in experiments 1 and 2, respectively, was designated the spinal sympathetic reflex index.

(C and D) Overall variance explained by PCA reveals separation between SCI animals treated with saline and pGBP. Large outlined symbol, mean of each group; ellipses, 99% confidence interval.

(E and F) Each subject is given a score for PC1 to assess the effect of treatment (E) and treatment and time post-injury (F) on the spinal sympathetic reflex index.

(E) Student's two-sided t test, n = 14–16 mice/group; $^{a}p < 0.05$, mean ± SEM.

(F) Two-way ANOVA with Bonferroni post hoc tests; n = 6–11 mice/group; $^{a}p < 0.0001$ for overall treatment effect; $^{b}p < 0.0001$ for GBP groups (red) compared with equivalent time points in the saline (blue) groups, mean ± SEM.

See also Figure S8.

KEY RESOURCES TABLE

REAGENT or RESOURCE	SOURCE	IDENTIFIER
Antibodies		
Rabbit-anti-mouse α2δ-1 (1:500)	Sigma-Aldrich	C5105; RRID: AB_258885
Hamster-anti-mouse CD3e (1:500)	BD Biosciences	550277; RRID: AB_393573
Rat-anti-mouse-CD45R (1:500)	Bio-Rad	MCA1258G; RRID: AB_323211
Rabbit-anti-mouse-CGRP (1:500)	Sigma-Aldrich	C8198; RRID: AB_259091
Rabbit-anti-mouse FosB (1:500)	Abcam	ab184938; RRID: AB_2721123
Chicken-anti-mouse GFP (1:500)	Aves Labs	GFP-1020; RRID: AB_10000240
Rabbit-anti-mouse Homer1 (1:400)	Synaptic Systems	160 003; RRID: AB_887730
Rabbit-anti-mouse TSP4 (1:200)	Ray Biotech	144-64382-50; RRID: AB_2858251
Guinea pig-anti-mouse VGlut2 (1:1000)	Millipore	AB2251-l; RRID: AB_2665454
Alexa Fluor 488 Goat-anti-Rabbit IgG (1:500)	Thermo Fisher Scientific	A-11008; RRID: AB_143165
Alexa Fluor 546 Goat-anti-Rabbit IgG (1:1000)	Thermo Fisher Scientific	A-11035; RRID: AB_143051
Alexa Fluor 488 Goat-anti-Rat IgG (1:1000)	Thermo Fisher Scientific	A-11006; RRID: AB_2534074
Alexa Fluor 568 Goat-anti-Guinea pig IgG (1:1000)	Thermo Fisher Scientific	A-11075; RRID: AB_141954
Alexa Fluor 456 Goat-anti-Hamster IgG (1:500)	Thermo Fisher Scientific	A-21111; RRID: AB_2535760
Alexa Fluor 488 Goat-anti-Chicken IgG (1:500)	Thermo Fisher Scientific	A-11039; RRID: AB_142924
Bacterial and virus strains		
Bartha strain pseudorabies virus-GFP	NIH Center for Neuroanatomy with Neurotropic Viruses (CNNV)	PRV-152
Chemicals, peptides, and recombinant proteins		
Gabapentin	Millipore Sigma	PHR1049
Fluoro-Gold	Fluorochrome LLC	Fluoro-Gold
Bovine serum albumin	Thermo Fisher Scientific	BP1600-100
Immu-mount media	Thermo Fisher Scientific	9990414
DRAQ5 nuclear dye	Abcam	ab108410
Trizol	Thermo Fisher Scientific	15596018
Triton X-100	Sigma-Aldrich	9002-93-1
Tissue-Tek OCT	VWR	25608-930
Critical commercial assays		

REAGENT or RESOURCE	SOURCE	IDENTIFIER
Fast SYBR Green qPCR mastermix	Thermo Fisher Scientific	4385612
Deposited data		
Raw and analyzed data	Open data commons for spinal cord injury	DOI: https://doi.org/10.34945/F5V30C
Experimental models: organisms/strains		
Mouse: C57BL/6J	The Jackson Laboratory	000664
Mouse: 129SVE α2δ-1 overexpressing transgenic	Li et al., 2006	N/A
Mouse: 129SVE α2δ-1 wildtype littermate	Li et al., 2006	N/A
Oligonucleotides		
Primer: TSP4 Forward: 5′-TGTTTCCGAGGT GTCCGATG-3′	This paper	N/A
Primer: TSP4 Reverse: 5′-GGAGCCAAATTCACACAGCG-3′	This paper	N/A
Primer: 18 s Forward: 5′-TTCGGAACTGAGGCCATGAT-3′	This paper	N/A
Primer: 18 s Reverse: 5′-TTTCGCTCTGGTCCGTCTTG -3′	This paper	N/A
Software and algorithms		
GraphPad Prism 8.0.2	GraphPad Software; https://www.graphpad.com/	SCR_002798
Microsoft Excel	Microsoft; https://www.microsoft.com/en-us/microsoft-365/excel	SCR_016137
Leica application suite (LAS X)	Leica; microsystems.com/products/p/leica-las-x-ls/	SCR_013673
Fiji/ImageJ 2.0.0	NIH; https://imagej.nih.gov/ij/download.html	SCR_002285
Imaris 8.1	Bitplane; https://imaris.software-free-trial	SCR_007370
MIPAR	MIPAR; https://www.mipar.us/	N/A
Dataquest	DSI https://www.datasci.com/products/software	N/A
MATLAB	MathWorks; https://www.mathworks.com/products/matlab/	SCR_001622
R 4.0.2	https://www.r-project.org/	N/A
RStudio 1.2.5003	https://rstudio.com/	N/A
prcomp	https://www.rdocumentation.org/packages/stats/versions/3.6.2/topics/prcomp	N/A
Other		
Bruker timsTOF Pro HPLC-MS/MS with Ion Mobility	Bruker	Bruker timsTOF Pro HPLC-MS/MS with Ion Mobility
4-French, 60 mm balloon-tipped catheter (Swan-Ganz monitoring catheter model)	Edward Life Sciences	116F4
DSI PhysioTel PA-C10 Pressure Transmitter for Mice	Data Sciences International	PA-C10
PhysioTel HD rodent telemetry receiver	Data Sciences International	PhysioTel HD receiver
PhysioTel HD rodent telemetry matrix 2.0	Data Sciences International	PhysioTel HD matrix 2.0